# Erbium BEC in an Optical Box Potential

## PhD in Physics - First Year Report

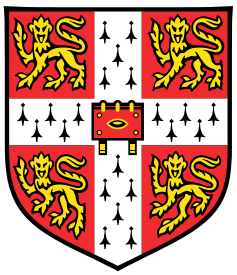

**Milan Krstajic**

Supervisor: **Dr Robert Smith**

Department of Physics
University of Cambridge

July 2018

# Declaration

I hereby declare that except where specific reference is made to the work of others, the contents of this report are original and have not been submitted in whole or in part for consideration for any other degree or qualification in this, or any other university.

Milan Krstajic
July 2018

# Acknowledgements

First and foremost, I would like to thank my supervisor, Robert Smith, and the group leader, Zoran Hadzibabic, for giving me a valuable opportunity to continue my studies in their group. I am also grateful to Julian Schmitt, Christoph Eigen, Raphael Lopes, Jay Man, Jake Glidden, Konrad Viebahn and Matteo Sbroscia for numerous useful comments, suggestions, answers to questions and help with equipment. Next, I would like to thank the Student Workshop Supervisor, Kevin Mott, for his generous assistance in machining and repairing components for our apparatus. Also, I would like to thank Panagiotis Christodoulou, Lena Bartha, Maciej Galka and Jinyi Zhang for many interesting conversations and for contributing to the very pleasant atmosphere in the group. Very importantly, I would like to thank my colleague on the erbium experiment, Nathaniel Vilas, for his extensive contribution to the project and a very productive collaboration. Last but not least, I would like to thank the Part III students, Tanish Satoor and Tobias Schaich, for their help and contribution through their projects.

# Abstract

We are building a new experimental setup to produce a Bose-Einstein Condensate of erbium atoms in an optical box potential. The aim is to investigate the effects of long-range, dipole-dipole interactions on quantum gas systems. Erbium was chosen for the experimental species as it has one of the highest available magnetic moments ($7\mu_B$) among chemical elements, and methods for cooling it to quantum degeneracy have been developed, making it an ideal species for this task. We have designed a vacuum chamber for the experiment, implementing the standard laser cooling protocols(2D optical molasses for transversal cooling, Zeeman Slower and a Magneto-Optical Trap), followed by an optical dipole trap for trapping and transporting the atomic cloud into a glass 'science cell' which enables sufficient optical access to impose the optical box potential to the atoms. At this point, the majority vacuum chamber has been built and the optical systems for laser cooling are in the process of being set up. This report aims to cover the context and the basic theoretical background behind the planned research, the overview of the experimental design and the building efforts undertaken so far, and finally to describe the research projects that we have in plan. The final section also contains a timeline of all planned tasks for the duration of my PhD course.

# Table of contents

# Chapter 1

# Introduction

## 1.1 Overview of Ultracold Atom Systems

In the past two decades, ultracold atom experiments have established themselves as ideal test beds for theoretical models from condensed matter and many-body quantum mechanics. Following breakthrough research on the subject of laser cooling [1], a degenerate quantum gas of bosons, the Bose-Einstein Condensate (BEC), was created in 1995 at JILA [2] and shortly after that at MIT [3]. Reaching quantum degeneracy in a fermionic system followed in 1999 [4]. With these achievements the ground was laid for experiments that can probe fundamental aspects of many-body quantum systems and simulate various physical systems of interest in order to put theories to the test. The multitude of available tools and methods now enables controlling the strength of interactions between atoms and confining atoms in various types of trapping potentials. Furthermore, recent developments in laser cooling expanded the spectrum of elements that can be condensed (Figure 1.1), including some elements with very high magnetic moments (chromium [5], erbium [6], dysprosium [7]). This adds a new dimension to experiments that can be realized, introducing long-range and anisotropic, dipole-dipole interactions (DDI) on top of the short-range, Van der Waals interactions present in all atomic species.

Traditionally, experiments are performed on ultracold atomic gases that are confined in (approximately) harmonic trapping potentials. This is the case since a trap of any functional form (excluding a very limited number of exceptions) can be well described with a quadratic function in the region around an extremum. For example, traps are often realised by using Gaussian laser beams to induce a light shift potential for the atoms. This situation does not reflect the continuous translational symmetry that many systems posses, and also limits the amount of information accessible through measurement, as a some quantities have spatially dependent values. This problem was solved by placing the atoms in the *optical box potential*,

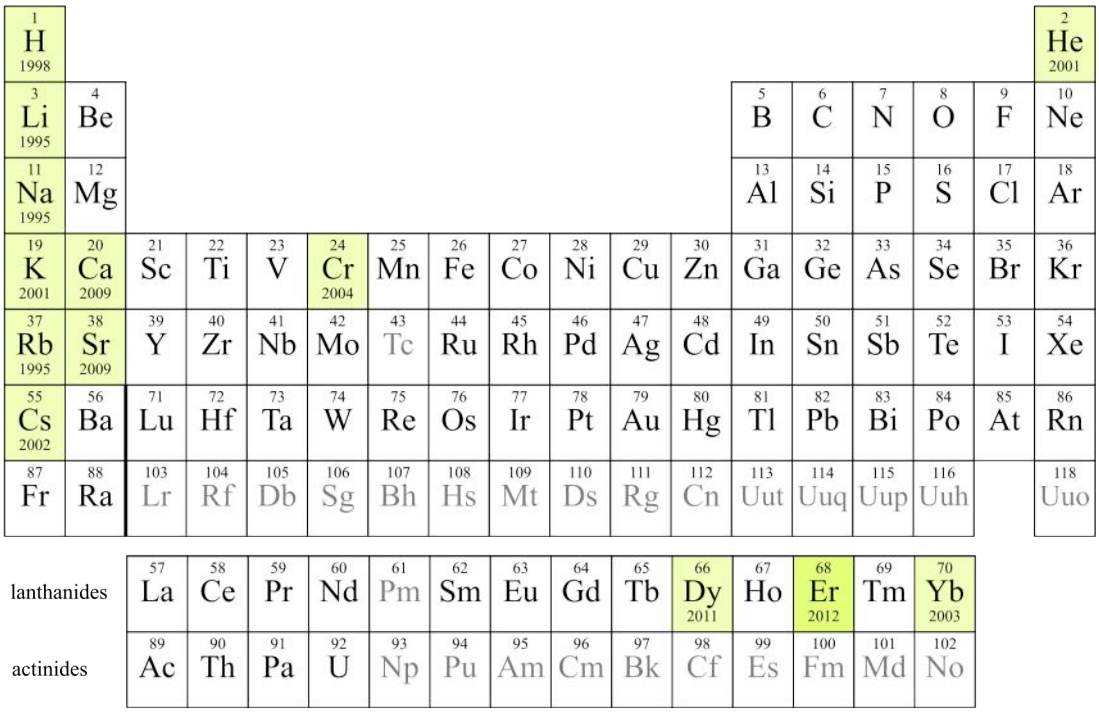


Fig. 1.1 The periodic system of chemical elements with the elements that have been condensed into a BEC being highlighted, also stating the year in which it was succeeded

first implemented in the Hadzibabic group at Cambridge University [8]. This technique cleared the way for many interesting topics to be examined, including the dynamics of passing through a phase transition at a finite rate [9], weak collapse in a BEC [10] and turbulence in a quantum gas [11].

## 1.2 Properties of Erbium

Erbium is a rare-earth element located in the *lanthanides* section of the periodic table. It was discovered in a sample of gadolinite ore by Carl Gustav Mosander in 1843. Its name (along with the names of terbium, ytterbium and yttrium) is derived from the name of the mine from which the ore originated - Ytterby. By appearance, erbium is a pale, silvery metallic substance, that easily oxidises and hence usually covers itself with a layer of oxide when exposed to air. It has the atomic number of $Z = 68$, and the average atomic mass of $A = 167.26$ *amu*. It naturally appears in six stable isotopes, five of them bosonic as shown in the Table 1.1.

| Isotope | $^{162}Er$ | $^{164}Er$ | $^{166}Er$ | $^{167}Er$ | $^{168}Er$ | $^{170}Er$ |
|---|---|---|---|---|---|---|
| Abundance | 0.14% | 1.61% | 33.6% | 23.0% | 26.8% | 15.0% |
| Statistics | boson | boson | boson | fermion | boson | boson |

Table 1.1 Abundances and statistical types od different erbium isotopes

### 1.2.1 Electronic Configuration and Transitions

The electronic configuration of erbium is $\left(1s^2 2s^2 2p^6 3s^2 3p^6 4s^2 3d^{10} 4p^6 5s^2 4d^{10} 5p^6\right) 6s^2 4f^{12}$ or using the noble gas configuration shorthand $[Xe]\,6s^2 4f^{12}$. This situation with valence electrons in a filled $6s$ level and partially filled $4f$ level is known as *submerged shell* configuration. Such an electronic shell is the reason behind the high magnetic moment of erbium. The two holes in the $4f$ contribute to the total angular momentum of $J = 6$ in the ground state.

The complicated electronic structure is also reflected in the very rich spectrum of electronic excited states (Figure 1.2(a), taken from [12]). Looking at the electronic-dipole transitions that couple the ground state with excited states, we can identify several transitions of interest for atomic physics purposes, covering a range of line widths, from wide (30 $MHz$) to ultra-narrow (2 $Hz$). Two transitions of particular interest for our experiment are the ones at 401 $nm$ and 583 $nm$ (Figure 1.2(b)) with linewidths of 29.7 $MHz$ and 190 $kHz$ respectively. The 401 $nm$ transition is the most prominent transition in erbium that is very convenient for initial stages of laser cooling and also has the leading order influence on the atomic polarizability, relevant for optical trapping. The yellow transition, at 583 $nm$, being reasonably narrow, is well suited for the Magneto-Optical Trap (MOT), giving a very low Doppler Temperature of approximately five microkelvin. The relevant properties of these two transitions are shown below in the Table 1.2.

| Transition | Blue | Yellow |
|---|---|---|
| Wavelength | $400.97nm$ | $582.84nm$ |
| Natural Linewidth | $29.7MHz$ | $190kHz$ |
| Doppler Temperature | $714\mu K$ | $4.6\mu K$ |
| Recoil velocity | $6.0\frac{mm}{s}$ | $4.1\frac{mm}{s}$ |
| Saturation Intensity | $60.3\frac{mW}{cm^2}$ | $0.13\frac{mW}{cm^2}$ |

Table 1.2 Useful parameters for the *blue* and the *yellow* transitions

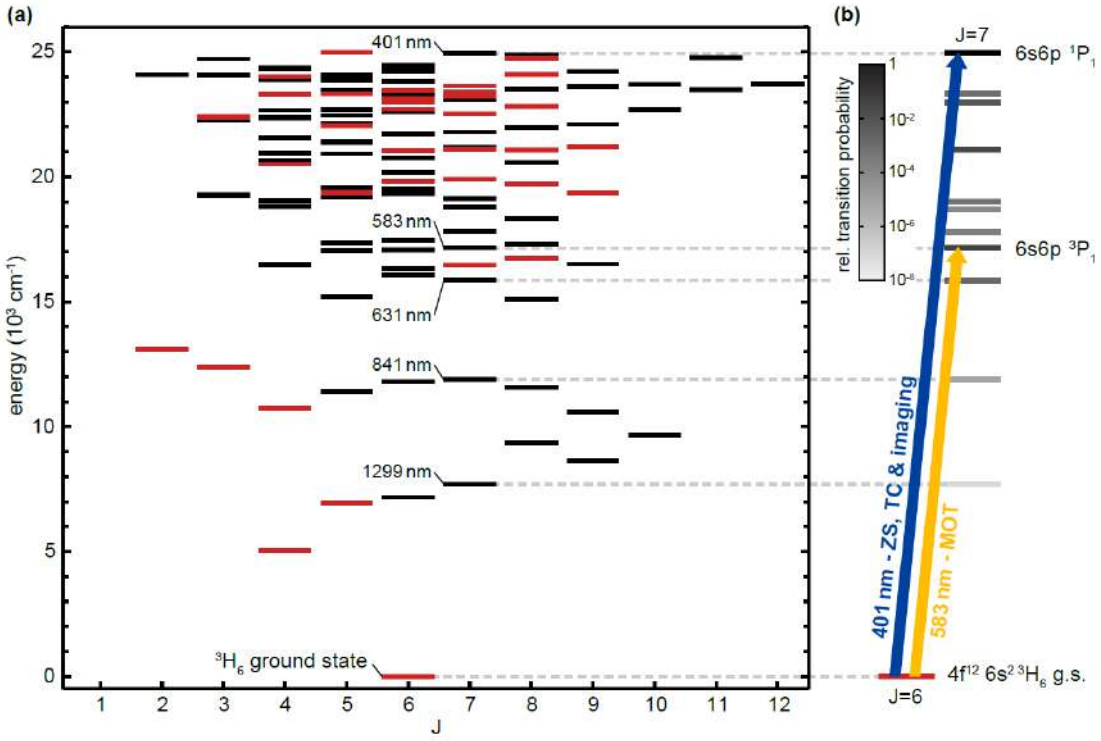


Fig. 1.2 (a) The diagram containing electronic energy levels of erbium, showing their energy, electronic angular momentum, $J$, and pairity. (b) An excerpt highlighting the two transitions used for laser cooling in our experiment, at 401 *nm* and 583 *nm*; figure taken from [12]

### 1.2.2 Magnetic Properties of Erbium

Elements with the largest magnetic moments can be found within lanthanides. Dysprosium and terbium lead the charts with $\mu = 10\mu_B$, followed by holmium, europium and erbium with $8\mu_B$, $7\mu_B$ and $7\mu_B$ respectively (here $\mu_B = \frac{e\hbar}{2m_e}$ is the Bohr magneton). As mentioned in the previous subsection, erbium owes its magnetic moment to the two unpaired electrons (*i.e.* holes) in the $4f$ sub-shell. In situations like the submerged shell configuration, the appropriate spin-orbit coupling scheme to apply is a special type of *jj*-coupling, called $J_1J_2$-coupling. The two '$J$'s' in this picture are the angular momenta of the submerged $4f$ shell and the outer valence electrons. Both the submerged shell electrons and the valence electrons here are first $LS$-coupled to give $J_1$ and $J_2$, and then the two $J$'s are coupled together. In the ground state, the two valence $6s$ electrons are in the $L = 0$ and $S = 0$ state, and the $4f$ electrons give an overall $^3H_6$ state with $L = 5$, $S = 1$ and $J = 6$, which also corresponds to the final coupled state. The Landé $g$-factor for this state can be theoretically calculated as:

$$g_J = 1 + (g_S - 1)\frac{J(J+1) - L(L+1) + S(S+1)}{2J(J+1)} = 1.1670533 \tag{1.1}$$

This doesn't include several known corrections, that can yield a value much closer to the actual experimentally measured value of $g_J = 1.163801(1)$. Knowing the Landé $g$-factor it is possible to calculate the magnetic moment of the given fine structure state, given by the value of $m_J$:

$$\mu = m_J g_J \mu_B \tag{1.2}$$

From here, we see that the total magnetic moment of an erbium atom in its ground state is $\mu\,(m_J = 6) = 6.982806(6)\mu_B$.

The two excited states corresponding to the optical transitions used in the experiment, both having $J = 7$, are:

- 401 nm exc. state : $[Xe]\,4f^{12}\left({}^3H_6\right)6s6p\left({}^1P_1\right)(6,1)_7$
- 583 nm exc. state : $[Xe]\,4f^{12}\left({}^3H_6\right)6s6p\left({}^3P_1\right)(6,1)_7$

with the Landé $g$-factors of $g_J = 1.160$ and $g_J = 1.195$ respectively. These values are important as the Zeeman shift of a given transition $\left(J^g, m_J^g\right) \rightarrow (J^e, m_J^e)$ induced by the magnetic field $B$ is calculated according to:

$$\Delta E_{Zeeman} = \left(m_J^e g_J^e - m_J^g g_J^g\right)\mu_B B \tag{1.3}$$

## 1.3 Project Goals

The centrepiece of our experimental effort is creating a dipolar BEC in a uniform trapping potential. We believe that the translational symmetry of the optical box is crucial for accessing the full flavour of the physics that stems from the long-range nature of the interatomic forces. Once the core of the experimental setup is completed, we will embark on the exploration of phenomena that are expected to occur in dipolar quantum gases, starting from roton physics [13], and following on to supersolidity [14]. Furthermore, we plan to explore the influence of long-range interactions in various scenarios that have already been attractive subjects in the field of ultracold gases, including driven [11] and quenched [9] systems. Finally, the long term project plan predicts the addition of a second atomic species, most probably potassium, to expand the range of physical models that we can simulate. These will, among other things, include subjects relevant to quantum information, like qubit decoherence control [29] [30].

## 1.4 Report Outline

The following chapter offers an overview of the physics of ultracold atomic systems relevant for this experiment. Chapter 3 will describe various aspects of the experimental design, Chapter 4 outlines the efforts, encountered issues and progress in the process of setting up the experiment up to the current state, and finally, Chapter 5 describes the building work and projects planned to be done on this experiment, focusing on the ones in the near future.

# Chapter 2

# Ultracold quantum gasses - Theory

## 2.1 Laser Cooling

Laser cooling is the key ingredient in reaching ultra low temperatures required for quantum degeneracy in atomic gases. The method relies on the scattering force present when the atoms are placed in a laser beam. This force is established by absorbing photons from the laser beam and then emitting them in a random direction in space. As the momentum transfer due to the absorption events is directed along the beam direction, whereas the momentum transfer linked to emission averages to zero over many events, the effective force due to photon scattering acts along the direction of the laser beam. To make this into an applicable scheme, one has to combine counter-propagating beams and make use of the Doppler effect by setting the appropriate detuning of the laser frequency with respect to the atomic transition. By keeping the lasers red-detuned, the atoms will preferentially absorb from the laser beam towards which they are moving, making the scattering force always directed opposite to their velocity.

The scattering force can be expressed as the product of the photon momentum and the scattering rate, so given the laser beam with the wavevector $k$, Rabi frequency $\Omega$ and detuning $\delta$ with respect to the atomic transition of width $\Gamma$, the scattering force is:

$$F_{Scatt} = \hbar k \frac{\Gamma}{2} \frac{\frac{\Omega^2}{2}}{\delta^2 + \frac{\Omega^2}{2} + \frac{\Gamma^2}{4}} \tag{2.1}$$

In practice, it is useful to use laser intensity in the equation instead of the Rabi frequency, so with the help of the expression $\frac{I}{I_{sat}} = \frac{2\Omega^2}{\Gamma^2}$, we can obtain:

$$F_{Scatt} = \hbar k \frac{\Gamma}{2} \frac{\frac{I}{I_{sat}}}{1 + \frac{I}{I_{sat}} + \frac{4\delta^2}{\Gamma^2}} \tag{2.2}$$

In the situation where the atoms are placed in a pair of counter-propagating beams, the effective detunings are different for the two beams because of the Doppler effect, $\delta_{\pm} = \delta \pm kv$. Then the effective force is the sum of the scattering forces from the two beams. For small velocities ($kv \ll \delta$), the scattering force has the form of a viscous force:

$$F_{Scatt} = -\alpha v = -4\hbar k^2 \frac{I}{I_{sat}} \frac{-\frac{2\delta}{\Gamma}}{\left(1+\frac{4\delta^2}{\Gamma^2}\right)^2} \tag{2.3}$$

In order to provide cooling along all three spatial directions, three pairs of counter propagating beams are usually used. The ultimate limit for the low temperature that can be reached with this method is called the Doppler temperature and originates from the shot noise in the absorption and the random walk in the velocity space due to spontaneous emission. The Doppler temperature is given by:

$$T_D = \frac{\hbar\Gamma}{2k_B} \tag{2.4}$$

A laser cooling technique, that is able to cool gases to sub-Doppler temperatures also exists - Sisyphus Cooling. It is based on a spatially varying polarization profile of the cooling beams combined with using multiple transitions from the same manifold.

### 2.1.1 Zeeman Slower

In many cold atom experiments, the atoms are loaded into the system from a high temperature oven. The oven is usually equipped with a set of apertures, producing a fairly collimated beam of atoms. As the typical oven temperatures used in these experiments correspond to velocities of several hundreds of meters per second, it is necessary to slow these down considerably in order to load the MOT successfully. Typical MOT capture velocities are between several and few tens of meters per second. The commonly used method for slowing down a collimated beam of atoms is a so called Zeeman Slower (ZS). It relies on the light scattering force from a laser beam counter-propagating with respect the atomic beam, and the Zeeman effect to keep the atoms resonant with the light once they start slowing down. The key feature of this method is an electromagnetic coil creating the magnetic field of an appropriate profile that cancels the Doppler shift along the deceleration path of the atoms. The following heuristic treatment can explain the basic principles - if we assume that the field profile is designed such that it keeps the laser detuning, and hence the scattering force, constant, the motion of a given atom can be described with the equation:

$$v_0^2 - v(x)^2 = \frac{2x}{m}\hbar k \frac{\Gamma}{2}\frac{s}{1+s+\frac{4\delta^2}{\Gamma^2}} \tag{2.5}$$

Where $\delta = \delta_0 + kv - \mu B$ is the effective detuning that is kept constant, and $\mu$ is the magnetic moment of the atom. The magnetic field should then follow the profile of the velocity $B(x) = \hbar\frac{\delta_0 - \delta + kv(x)}{\mu}$. The dependence of the velocity on position then has the form:

$$v(x) = v_0\sqrt{1 - \frac{x}{x_0}} \tag{2.6}$$

with $x_0 = \frac{2\hbar k}{mv_0^2}\frac{\Gamma}{2}\frac{s}{1+s+\frac{4\delta^2}{\Gamma^2}}$ being the stopping length. The above equation immediately gives the required field profile:

$$B(x) = B_{bias} + B_0\sqrt{1 - \frac{x}{x_0}} \tag{2.7}$$

$$B_{bias} = \hbar\frac{\delta_0 - \delta}{\mu} \tag{2.8}$$

$$B_0 = \frac{\hbar k v_0}{\mu} \tag{2.9}$$

Here $v_0$ represents the capture velocity, and all the atoms below it will also be slowed down, once they reach the position of the slower where they become resonant. In order to increase robustness of the slower $\delta$ should be kept at a finite negative value, which will decrease the capture velocity and the efficiency, but will reduce the influence of field imperfections and scattering random noise. The ZS efficiency is defined as the ratio of the actual and the maximum attainable ZS deceleration, $a_{ZS(max)} = \frac{\hbar k\Gamma}{2m}$:

$$\eta = \frac{a_{ZS}}{a_{ZS(max)}} = \frac{s}{1+s+\frac{4\delta^2}{\Gamma^2}} \tag{2.10}$$

and the ZS will exhibit robust behaviour for $\eta \leq \frac{2}{3}$ [12].

### 2.1.2 Magneto-Optical Trap

The MOT combines the Doppler and the Zeeman effect to employ the light scattering force for trapping and cooling simultaneously. Introducing a variable magnetic field, with gradients along all three directions, causes the light scattering force to have a component directed towards the centre of the trap. Based on the parameters, each MOT has a capture velocity, $v_c$, that determines the cut off above which the atoms cannot be trapped. In order to increase the

capture velocity of a given trap, it is necessary to start from a large detuning and than scan the detuning down towards the ideal value (this approach is called the *compressed MOT*).

## 2.2 Optical Trapping

When atoms are subjected to a non-resonant light field, their potential energy changes through the AC-Stark effect. That effect can be simply explained through the *dressed state* picture, where the eigenstates of the atom in the light field are original eigenstates mixed with small proportions of other states. All the states corresponding to transitions for which the laser is blue/red detuned increase/decrease the energy of the atom. For a two level system, with the far detuned light field, the energy shift is given as:

$$\Delta E = \frac{\hbar \Omega^2}{4\delta} \tag{2.11}$$

Often, the magnitude of the shift of a given atom species is described through polarizability, $\alpha$, defined by:

$$\Delta E(\omega) = -\frac{1}{2\varepsilon_0 c} I\alpha \tag{2.12}$$

In general, the polarizability has a tensorial character, and depends on the angle between the quantisation axis and the polarisation of the light field, $\theta_p$ and the angle between the quantisation axis and the propagation direction of the light beam,$\theta_k$ (as defined in the inset of Figure 2.1). For erbium, in case when both of these angles are 90°, the polarization is shown in the Figure 2.1, originally from [15].

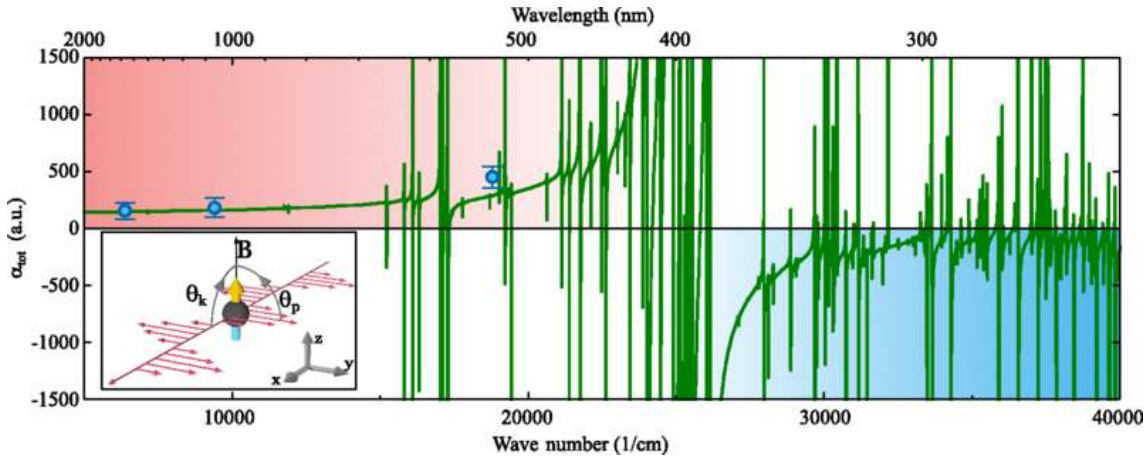


Fig. 2.1 The plot showing the atomic polarizability of erbium at different wavelengths for $\theta_k = \theta_p = 90°$, taken from [15]

From the above graph, it is clear that an attractive optical dipole trap (ODT) can be successfully created using wavelengths in the 1030 *nm*-1050 *nm* region, and a repulsive optical box potential may be set up using light close to 370 *nm*. The region of favourable ODT wavelengths is, of course, much wider, but given the availability of high power lasers, and the fact that an issue with trapping the fermionic isotope, $^{167}Er$ using the common ND:YAG laser at 1064 *nm* (Appendix D), we decided to restrict our search to the 1030 *nm*-1050 *nm* interval.

## 2.3 Bose Gas with Dipolar Interactions

In the well known case of scattering between alkaline atoms in ultracold bosonic gas systems, the scattering properties can be described using a single parameter - the scattering length, $a$. Because the energies involved are low, the atom interactions are dominated by the s-wave scattering, and well described by the pseudo-potential:

$$V_{cont.}(\mathbf{r},\theta) = \frac{4\pi\hbar^2}{m} a\delta(\mathbf{r}) \tag{2.13}$$

This behaviour stems from the short-range and isotropic nature of the Van der Waals (or dispersion) interactions, that take the form $U_{VdW} \sim \frac{c_6}{r^6}$.

In erbium, owing to the electronic structure, the DDI force is present in addition to the dispersion force, which is also no longer anisotropic. It turns out that the scattering can still be well described with a single scattering length at low energies, but in this case the process is not single channel, and the effective scattering length actually contains contributions from many scattering channels. A direct consequence of this is the very rich Feshbach spectrum [16] stemming from numerous states that take part in scattering processes. Due to this anisotropy, the dispersion potential is described by a spread of $C_6$ coefficients, described by $\Delta C_6$, which for erbium take values $C_6 = 1723 a.u.$ and $\Delta C_6 \sim 350 a.u.$, hence showing a significant degree of anisotropy. The second consequence of the DDI is the long range potential that is also present and takes the form:

$$U_{dd}(\mathbf{r}) = \frac{C_{dd}}{4\pi} \frac{(\mathbf{e}_1 \cdot \mathbf{e}_2) r^2 - 3(\mathbf{e}_1 \cdot \mathbf{r})(\mathbf{e}_2 \cdot \mathbf{r})}{r^5} \tag{2.14}$$

For magnetic dipoles, $C_{dd} = \mu_0 \mu^2$. The pseudo potential formalism can still be employed, but it no longer takes the simple $\delta$-function form. For example, in a gas of polarized dipolar atoms, the pseudo potential with dipolar interactions included can be written as:

$$V_{int}(\mathbf{r},\theta) = \frac{4\pi\hbar^2}{m} a_{eff}\,\delta(\mathbf{r}) + \frac{\mu_0\mu^2 m}{12\pi\hbar^2}\frac{1-3\cos^2\theta}{r^3} \tag{2.15}$$

A result relevant for the scope of the report is, for example, the dependence of this pseudo potential on the angle, $\theta$, between the polarisation axis and the line connecting the atoms, leads to the softening of the Bogoliubov dispersion relation, as described in the Section 5.1.1.

# Chapter 3

# Experimental Design

The primary goal of the design process is a setup that produces a BEC of erbium within the optical box and guarantees sufficient lifetime of the sample together with optical access for all the tools required by future investigative projects. Adding to that, it is necessary for the setup to be computer controlled, so the sample preparation measurement processes are automated, and for the magnetic fields within the experiment chamber to be stabilized to high precision. In order to fulfil these requirements, we have designed a vacuum chamber implementing tools for cooling and trapping the atoms, laser systems providing the necessary light, a set of electromagnets creating and actively stabilizing fields and a computer control system for automation.

## 3.1 Vacuum Chamber

The vacuum chamber, shown on the Figure 3.1, consists of two subsystems - the High Vacuum Section (HV) and The Ultra-High Vacuum Section (UHV). The HV section consists of the Erbium oven, serving as a source for the beam of erbium atoms, and the Transversal Cooling (TC) stage, being the first stage of laser cooling. It also incorporates a set of auxiliary viewports for atomic beam characterisation (BC) that can be employed for optimizing the flux in the atomic beam. Continuing down the path of the atoms, the UHV section is separated from the HV section by a gate valve and the Zeeman Slower tube, carrying the profile electromagnet coil, that simultaneously acts as a differential pumping tube. The UHV section is centred around the MOT chamber, and has the Zeeman slower mirror branch, and the Science Cell branch, together with some pumping ports. Finally, there is a valved-off branch that is assigned for the future expansion of the experiment involving the addition of a second atomic species.

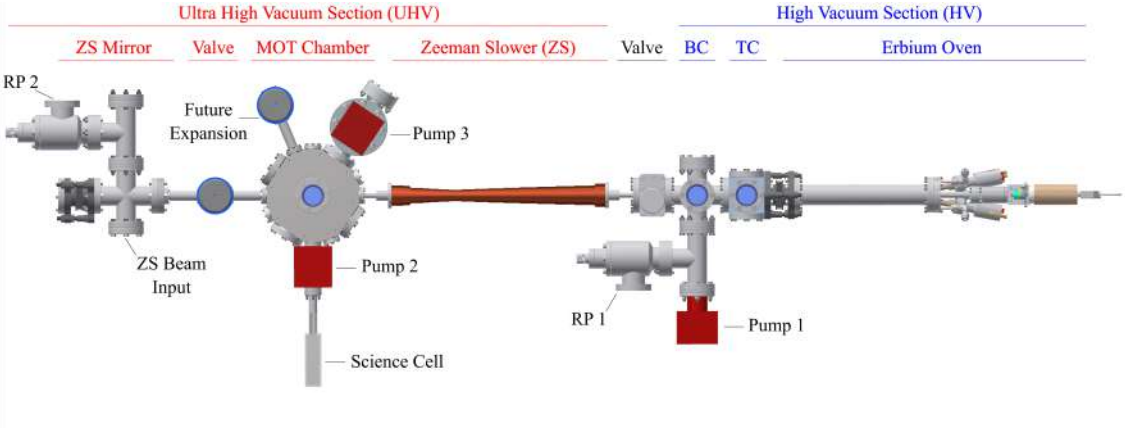


Fig. 3.1 Full vacuum system: TC - Transversal Cooling; BC - Beam characterisation; RP1 and RP2 - ports for attaching the rough pumping systems

In order to get a better insight into the requirements that laser cooling sets on the vacuum chamber, and to assist some decisions, a computer simulation of the atomic beam propagation and slowing has been written. The results obtained in the simulation were used throughout the design process. The model behind the simulation and the obtained results are presented in Appendix A.

### 3.1.1 Erbium Oven

The source of erbium in our experiment is an effusion cell oven [1]. It consists of a tantalum crucible (melting point of tantalum is $3017°C$), housing the solid erbium material, that is heated to high temperatures to increase the vapour pressure, and has a system of two heated apertures that produce a collimated atomic beam. The region of the crucible with the second aperture, the *hot lip*, can have its temperature independently controlled by a separate heater filament. A shutter that can be operated via a mechanical feed-through is installed in front of the exit aperture of the oven. It can be used to block the atomic beam after the MOT loading process is completed.

The oven is mounted to the chamber via a port aligner to make sure that the atomic beam can be aimed down the Zeeman slower tube. Finally, at the entrance to the TC cube, an additional aperture in the form of a copper gasket with an 8 *mm* internal diameter through hole, was installed to remove the atoms that have already diverged to far from the centre of the beam to successfully pass through the system. According to the computer simulation (Appendix A), the aperture is crucial for obtaining a good efficiency of transversal cooling, because the atoms that are stopped on in would absorb a significant portion of TC light (the

[1] Dual Filament Cell, model DFC-40-10-WK-2B-SHE, from *Createc*

atoms that go through, that make up $\approx 4\%$ of the total atomic flux, already absorb several percent of all the available photons - Figure A.4, and also [17]). As the material deposition rate on this aperture is expected to be fairly high, it is implemented in the form of a custom copper gasket at the flange connection between the port aligner and the cube, so it can be easily replaced in case a significant amount of erbium accumulates on it.

### 3.1.2 Transversal Cooling

The transversal cooling stage consists of a DN40CF[2] cube with four viewports along the transversal directions. The viewports allow for collimated beams of maximum size of 35 *mm* to be sent onto the atomic beam. Further to that, a 6-way cross is fitted after the cube, carrying three auxiliary viewports, and a flange leading to the vacuum pump and the rough pumping port with an angle valve. The TC viewports are coated with a broadband anti-reflection coating covering the range of wavelengths between 400 *nm* and 767 *nm*, whereas the three viewports on the cross have an unknown coating with $\sim 94\%$ transmission for both surfaces together at the wavelength of 401 *nm* (taken from an old apparatus) [3].

Based on the results obtained in the atomic beam computer simulation (Appendix A, Figure A.4), for oven temperatures up to $\approx 1100°C$, it is generally favourable to retro-reflect the TC beams, as the gain from having twice the power trumps the loss in the beam power due to absorption.

### 3.1.3 Zeeman Slower

The Zeeman slower tube is an 8 *mm* ID differential pumping tube, with a 20 *mm* outer diameter, double wall structure on the outside that carries the electromagnet coils and allows for its water cooling. The full length of the ZS tube is about 56 *cm*, to have room for the 42 *cm* long ZS coil, two water inlet/outlet ports[4] and some clearance space around the flanges for accessing the bolt holes. Given its internal diameter and length, the ZS tube can also act as a differential pumping tube, providing a pressure differential of up to two orders of magnitude between the HV and the UHV section (according to the analysis in Appendix B). This ensures that we can reach desirable pressure levels in the UHV sections even if the outgassing rate from the erbium oven turns out to be high.

At the start of the Zeeman Slower tube, a gate valve is mounted to provide isolation between the two sections of the apparatus, in case the HV section needs to be vented for

[2] CF refers to flange connections obeying the *ConFlat* standard

[3] These viewports have been recycled from a vacuum chamber no longer in use

[4] $\frac{1}{4}$" Swagelok connections

maintenance purposes (e.g. refilling erbium material or removing excess metal deposited on the chamber walls). The flange connection to the MOT chamber is made from the low magnetic permeability stainless steel alloy (316 LN).

### 3.1.4 MOT Chabmer

The MOT chamber is the central part of the experimental apparatus. It connects the various parts of our setup and provides optical access for the MOT beams, optical transport, imaging and the Zeeman Slower beam (Figure 3.2). It is a solid block chamber, made from 316 LN stainless steel, with 12 flange connections (4x DN40CF & 8x DN16CF) in the horizontal plane and two DN40CF in the vertical plane. On its top and bottom side it has 20 *mm* deep grooves machined around the flanges to house the electromagnet coils. Also, it has eight holes, symmetrically arranged around the collar on each side, to act as support points for the chamber itself, as well as the optics and coils mounted around the chamber.

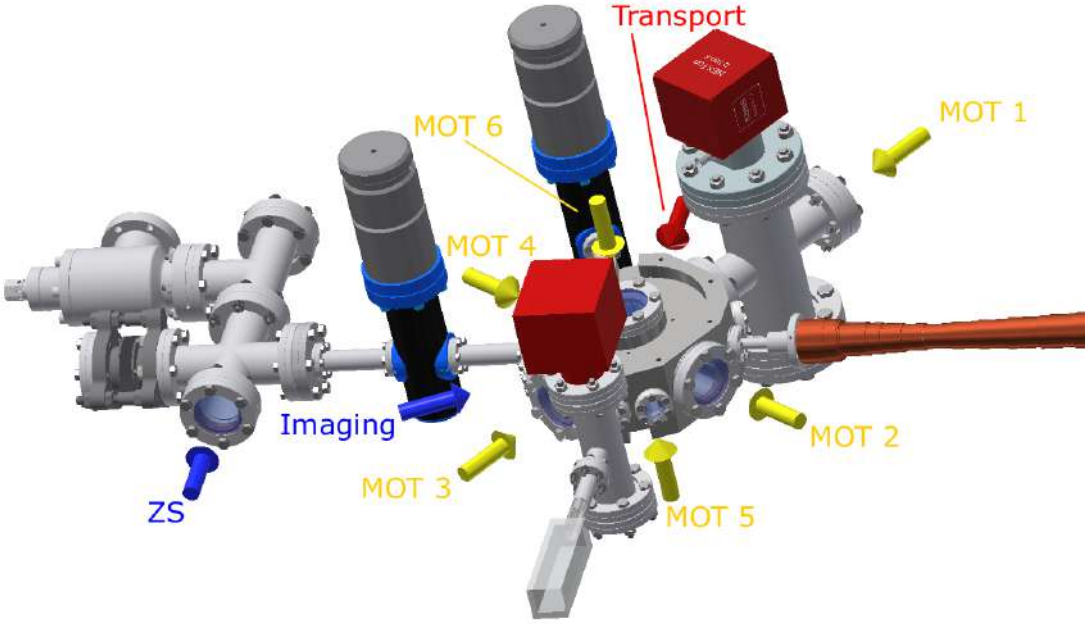


Fig. 3.2 Optical access to the MOT chamber: The six DN40CF viewports are intended for the MOT beams (two vertical and two horizontal MOT windows also offer the possibility of introducing a CDT beam). One pair of DN16CF viewports will be used for imaging and the DN16CF viewport opposite to the science cell is intended for transport

The MOT beam viewports have all been coated with broadband anti-reflection coatings. In order to retain flexibility for introducing a second ODT beam through one of the MOT viewports, creating a crossed-dipole trap (CDT), the MOT viewports were coated in pairs,

such that one pair can transmit 1064 *nm* light efficiently, whereas the other can transmit the 1550 *nm* light. All six viewports are also optimised for the wavelengths of 583 *nm* and 767 *nm* anticipating the addition of potassium as the second species.

The chamber is also fitted with a pair of AR coated[5] DN16CF viewports for imaging along one of the horizontal directions, and opposite to the science cell, an AR coated[6] DN16CF viewport for the optical transport beam.

### 3.1.5 Science Cell

A rectangular Boroflat glass cell will be fitted on one side of the MOT chamber to provide good optical access for performing the experiments. We decided not to AR coat the science cell as optical access will be required from various directions over a very wide interval of wavelengths. In that case, coating the cell which improves performance for certain beams will necessarily impair the reflection properties for some other beams.

In order to achieve a good atomic cloud lifetime in the Science Cell, we decided to include a reducer cross with a vacuum pump between the MOT Chamber and the Science Cell. This sets the total distance over which the atoms need to be transported between 25 *cm* and 30 *cm* (depending on the exact dimensions of the science cell that we end up ordering).

### 3.1.6 Zeeman Slower Mirror

The ZS laser beam needs to be directed into the path of the atoms off a mirror, as the incoming atoms are being deposited on the first surface they encounter, precluding the usage of a viewport for this purpose (according to quick estimates, a mono-layer of erbium atoms would be form on a viewport after a day of operating the experiment). On the other hand, the deposition of erbium on the mirror does not affect its performance significantly, as observed on similar experiments [12] [18].

The mirror is a full aluminium mirror with a UV-enhanced polished and coated surface[7]. It is fixed on a post resting on a flange mounted on a port aligner, giving an additional degree of freedom for coarse alignment (Figure 3.4b). This section is also valved off in case mirror maintenance is required at some point during the operation of the experiment.

[5] broadband AR coating 400 *nm*-767 *nm*

[6] broadband AR coating 1064 *nm*-1570 *nm*

[7] Custom mirror by Thorlabs, mirror surface and coating equivalent to F01 UV Enhanced Aluminium mirrors

### 3.1.7 Pumping

The pumping in the setup is provided by three combined NEG/Ion pump elements[8]. One pump rests in the HV section, and two pumps are placed in the UHV section. Rough pumping during the initial pump-down was performed with a turbo pump[9] backed with a scroll pump[10], through one of the two existing rough pumping ports (one at the HV section, and one at the ZS mirror branch).

As the part of the design process, the required pump strengths were estimated by representing the vacuum system using the molecular flow model and a set of assumptions regarding out-gassing and leak rates. In the model, the vacuum chamber is represented with an equivalent electrical circuit. The pumps are equivalent to grounding points with appropriate lead conductances corresponding to pumping speeds (in litres per second). The tubes and chambers, connecting different points in the setup, are then equivalent to resistors, and the leaks and out-gassing are entering the model as current sources. In this picture, voltages correspond to pressures in the system. The detailed analysis of our experimental system based on the molecular flow model is given in the Appendix B. In the analysis process, we considered several possible solutions for the pumping systems, based around the NEG/Ion pumps, and combinations of ordinary Ion pumps together with Ti-Sublimation Pumps.

According to the calculation that we have performed, we expect a pressure of $< 3 \cdot 10^{-11}$ *mbar* in the MOT chamber and $< 8 \cdot 10^{-12}$ *mbar* in the science cell. This should lead to BEC lifetimes that are sufficiently longer than the period of one experimental cycle (up to 10's of seconds).

## 3.2 Laser Systems

Our experiment employs multiple laser systems for cooling, trapping, transporting and imaging the atoms. The design of the blue and the yellow system (cooling lasers) is mostly finalized and portions have already been built. The transport system has been a subject of a project done by a Part III student [19], and it is conceptually thought out, but the exact design will be influenced by the particular laser used, that has not been purchased yet. The system for creating the optical box is yet to be designed, but the laser has been purchased, at the wavelength around 370 *nm*[11] as suggested in Section 2.2.

[8] 2x Nextorr D 100-5 and 1x Nextorr D 300-5 from SAES Getters

[9] Leybold Œrlikon Turbovac TW70H

[10] Leybold Œrlikon Scrollvac SC 5D

[11] Tunable system comprised of a MSquared Solstis Ti-Saphhire module with an MSquared ECD-X frequency doubler, pumped from a 8W Lighthouse Photonics Sprout G 532 *nm* laser

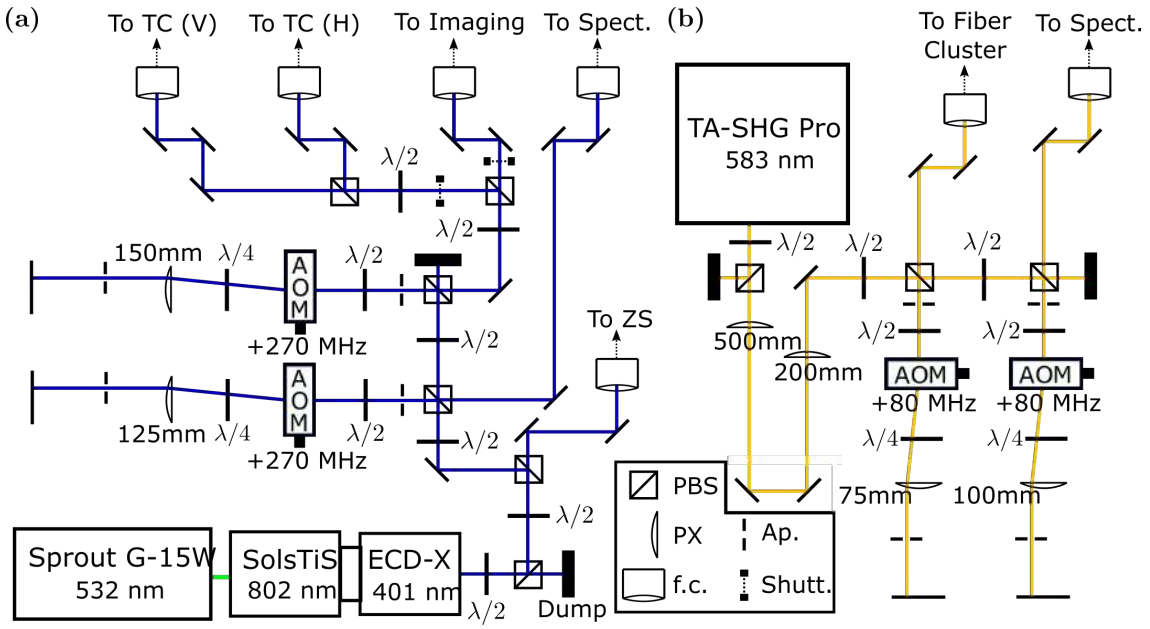


Fig. 3.3 (a) 401 *nm* laser distribution system: (b) 583 *nm* laser distribution system: Similarly to the blue laser system a pair of double pass AOM systems at 80 $MHz$ is used to detune the laser frequency away from resonance and then back to its proximity. This allows for the total detuning to be adjusted to anywhere in the range from 0 $MHz$ to ≈10 $MHz$ as required for the operation of the MOT

### 3.2.1 Blue laser

The blue laser at the wavelength of 401 *nm* is used for the initial laser cooling steps, the TC and the ZS, and for imaging. The source of the light is a frequency doubled[12] Ti-Sapphire[13] laser pumped from a solid state green laser[14]. The system is capable of outputting up to 2.1W of optical power at the wavelength of 401 *nm*.

As shown on Figure 3.3(a), the laser is locked 540 $MHz$ away from the atomic transition by detuning the spectroscopy beam using a double pass AOM[15] and the ZS light is picked off immediately after the laser output. Using another double pass AOM setup at the same frequency, the TC and imaging beams are detuned back to the vicinity of the atomic transition, with the ability to independently set this detuning. As TC and imaging are not used simultaneously, two shutters control to which branch the light intensity is fed to.

The Figure 3.4 shows the distribution optics to the cooling stages. The Zeeman Slower stage has a movable lens installed (Figure 3.4b), so that the beam can be focused down to

[12] MSquared ECD-X module
[13] MSquared SOLSTiS system
[14] 15W Lighthouse Photonics Sprout G, 532 *nm* laser
[15] Gooch & Housego AOMO 3270-125 Acusto-Optical Modulator at 270MHz

better match the profile of the ZS atomic beam (as suggested in [12]). The TC stage (Figure 3.4a) incorporates a set of spherical lenses that allow for the minor axis waist of the elliptical beam to be adjusted freely, followed by a cylindrical lens system that can be used to adjust the aspect ratio of the beam. Based on results obtained in the atomic beam simulation, it is favourable to 'mode-match' the cooling beam with the profile of the atoms that successfully pass through the ZS. Hence, the tunability of the beam size allows us to optimize the TC and ZS.

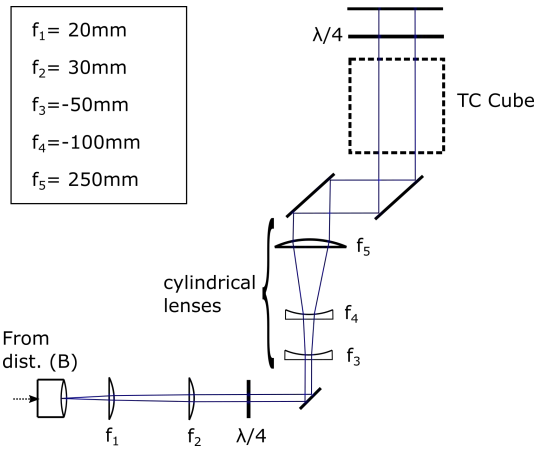


(a) TC distribution optics, showing the tunable lens systems used to change the size and the aspect ratio of the TC beams. The TC beams are retro-reflected into the chamber once they pass through it once

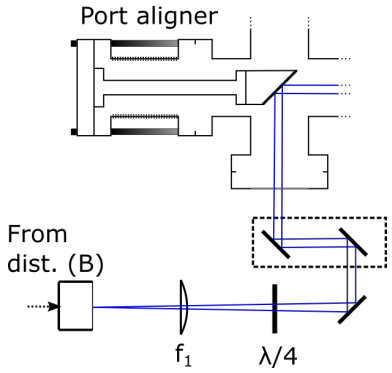


(b) ZS distribution optics incorporating a movable lens for slightly converging the ZS beam down the atomic beam, to better match the profiles.

Fig. 3.4

### 3.2.2 Yellow laser

The MOT is based on the narrow-line transition in erbium at 583nm having the linewidth of 190 $kHz$. The laser[16] provides about 700mW of laser available at its output, which is considerably more than it is needed for the MOT, given the low saturation intensity of the 583 $nm$ transition (see Table 1.2). The distribution optics breadboard is depicted on Figure 3.3(b), and the design of the fibre cluster that distributes the power to the six MOT beams is shown on Figure 3.5a.

In order to achieve Doppler limited cooling, it is essential to stabilize the laser frequency to a linewidth below the natural width of the transition. As for the blue laser, a Hollow Cathode Lamp (HCL) is used as a frequency reference.

[16]TOPTICA DL-TA-SHG-Pro diode laser with a tapered amplifier and a frequency doubling cavity

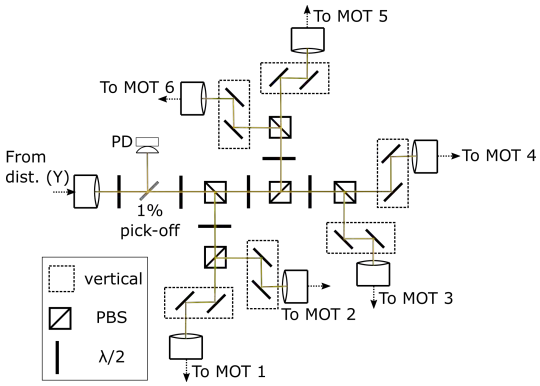


(a) MOT Fibre Cluster

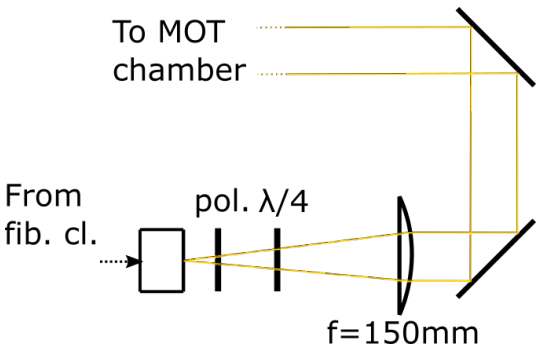


(b) MOT beam delivery optics

### 3.2.3 Modulation Transfer Spectroscopy

Both of the cooling lasers are locked using the same method called Modulation Transfer Spectroscopy (MTS). The method is thoroughly described in [20]. It is a Doppler-free spectroscopy method relying on four-wave mixing induced by an optical non-linearity. It gives a dispersion shaped error signal, with zero offset, making it convenient for feedback applications. We have set up an apparatus for MTS shown in Figure 3.6, using an erbium HCL[17] as the spectroscopy cell.

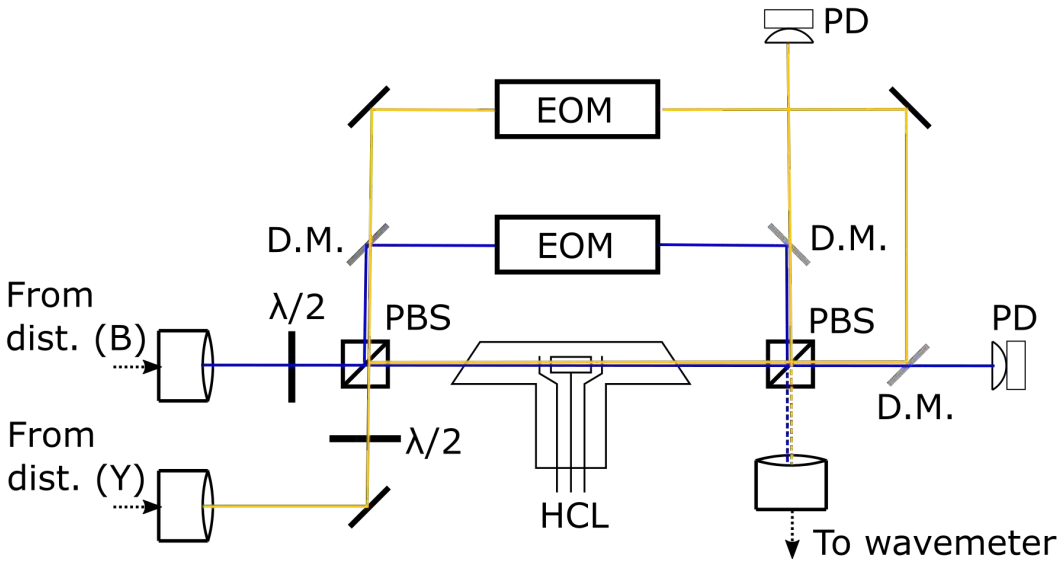


Fig. 3.6 Dichroic MTS setup working at 401 *nm* and 583 *nm*

[17] made by Heraeus

The signals that we have obtained for the 401nm line and the 583nm line are given in Figures 3.7a and 3.7b.

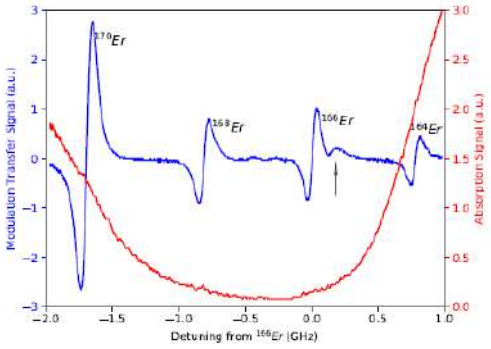


(a) 401 *nm* MTS signal

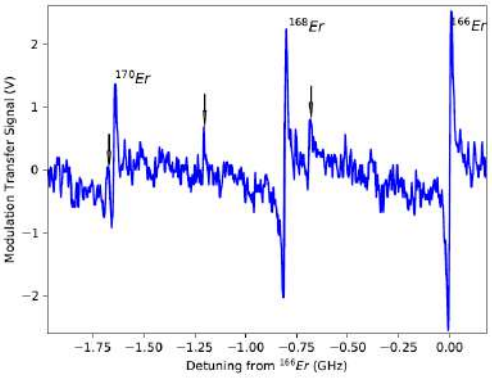


(b) 583 *nm* MTS signal

### 3.2.4 Transport

An infra-red laser of relatively high power will be used to provide the beam for the ODT. The ODT beam will be fed into the chamber using an optical system incorporating focus-tunable lenses[18]. With this setup, the focal position and the waist size of the ODT can be varied, allowing us to perform transport of the atoms from the MOT chamber to the Science Cell following the loading process from the MOT to the ODT. The pioneering implementation of this technique is given in [21]. In order to enhance the loading, an AOM has been installed into the ODT optical system, alowing us to laterally scan the ODT position at a high frequency, producing an effective potential of increased waist. This will provide better spatial overlap between the ODT potential and the atoms in the compressed MOT.

An open subject in discussion about choosing the exact wavelength used for the ODT beam. The availability of various laser systems puts wavelengths in the 1064 *nm* region in a favourable position, but there have been reports of problems with using 1064 *nm* for trapping the fermionic isotope of erbium. Based on an assumption about the loss mechanism that we have developed (Appendix D), we believe that a laser with the wavelength in the 1030 *nm*-1050 *nm* should not show the same type of problems.

[18]EL-16-40-TC-NIR from OptoTune

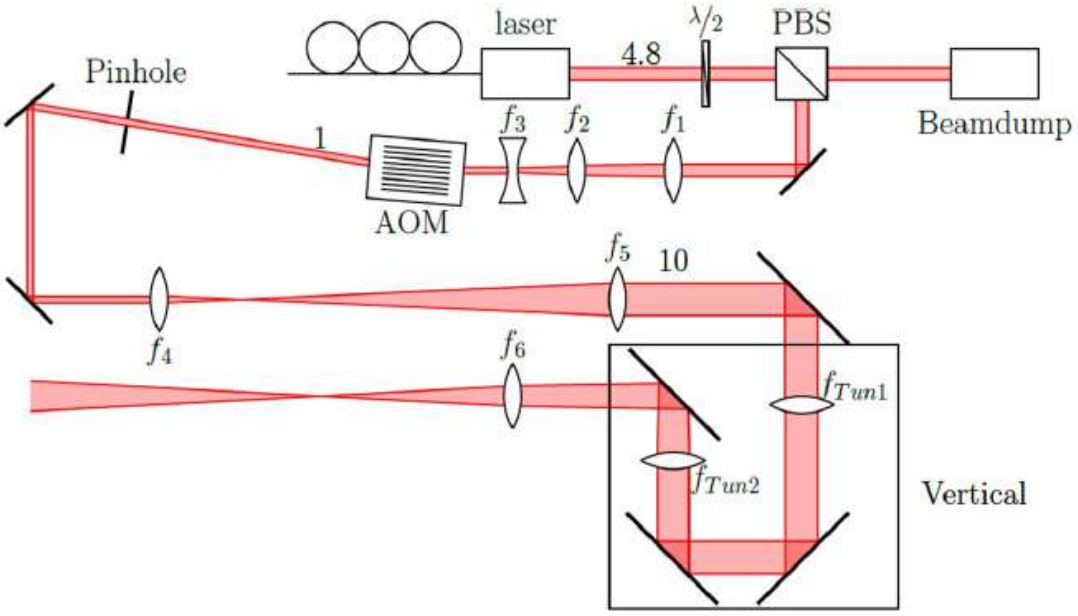


Fig. 3.8 Transport optical system, taken from [19]

## 3.3 Magnetics

Several experimental steps in our setup rely on providing adequate magnetic fields for the atoms. The Zeeman slower and the MOT require magnetic fields for shifting the optical transition frequency by the means of the Zeeman shift. In order to vary atomic scattering properties through Feshbach resonances, it is further needed to provide uniform fields stable within a miligauss. In order to create these fields our experiment is equipped with:

- The ZS coil, consisting of the bias coil and the profile coil. The bias coil is made from a single layer of 1 *mm* copper enamel wire along the full length of the slower. The profile coil is made from the same type of wire by varying the number of layers along the slower (Table 3.1). This coil system can provide the magnetic field directed along the Zeeman slower tube giving the ZS critical velocity up to 450 $\frac{m}{s}$.

| | Layer / Length[*mm*] | | | | | | | | | | | |
|---|---|---|---|---|---|---|---|---|---|---|---|---|
| | 1 | 2 | 3 | 4 | 5 | 6 | 7 | 8 | 9 | 10 | 11 | 12 |
| Bias | 420 | | | | | | | | | | | |
| Profile 1 (neg.) | 282 | 257 | 230 | 200 | 168 | 134 | 98 | 61 | 20 | 20 | 20 | 20 |
| Profile 2 (pos.) | 114 | 94 | 75 | 62 | 37 | 37 | 37 | 37 | 24 | | | |

Table 3.1 The structure of the Zeeman Slower coils, taken from [22]

- The Zeeman slower compensation coils, located just before and after the MOT chamber, along the ZS direction. These have the role of cancelling the field magnitude and gradient due to the ZS coils in the centre of the MOT chamber. These are rectangular profile coils wound from 1mm diameter copper enamel wire, each having 24 windings
- The MOT Gradient Coils - a pair of coils mounted above and below the MOT chamber in the anti-Helmholtz configuration, used to create the space-varying field within the MOT chamber necessary for establishing a MOT.
- MOT Chamber Feshbach Coils - a pair of coils in the Helmholtz configuration around the MOT chamber used to produce uniform fields within the chamber in order to address Feshbach resonances.
- Compensation Cage - a set of seven large rectangular coils, 24 windings each, mounted around the chamber and the future position of the science cell. It is designed to be used for active compensation of magnetic field noise, as well as for applying bias fields (e.g. during optical transport to maintain the polarisation if the atomic cloud)

The science cell, once it is installed, will have its own set of compensation coils which will allow for finer field stabilization. Further details about the magnetics will be available in [22].

## 3.4 Computer Control

In order to run the experiment in a synchronized manner, and also to automate acquiring experimental data, the full experimental system will be computer controlled through a National Instruments chassis[19]. It will house two analogue[20] and one digital output card[21], providing in total of 32 digital and 40 analogue independently controllable outputs. From the software side, the experiment will be controlled using the Cicero [23] sequence generator, communicating with the NI chassis via the Atticus server. The system will employ an FPGA chip[22] that provides the variable time-base signal for clocking the NI cards. By doing this the maximum sequence length or complexity is greatly increased by reducing the redundancy of the data fed into the cards' buffer.

[19] NI PXIe-1082 8-Slot PXI Express Chassis

[20] NI PXIe-6733 8 Channel, 16-bit Analog Output Card and NI PXIe 6738 32 Channel, 16-bit Analog Output Card

[21] NI PXIe-6536 32 Channel Digital Output Card

[22] XEM6001 from Opal Kelly Inc.

# Chapter 4

# Setting up the Experiment

This section will describe the progress made so far in building the experiment. The current state of the experiment is the following:

- The vacuum system has been assembled and leak-checking is in progress.
- The cooling laser systems are working, and the distribution optics is being set up.
- The optical transport setup has been tested as a standalone module. The design used should be implemented to the experiment in more or less the same form.
- Electromagnets for the Zeeman Slower and the compensation cage have been wound. The MOT chamber coils have been designed and we are waiting for the coil housing to be manufactured.
- Computer control hardware has been obtained and partially set up.

## 4.1 Vacuum System

The orders for the vacuum components were finalized in late February 2018. The majority of the components, including the custom chamber and the ZS tube, were ordered from Scanwel. The all metal valves were supplied by VAT valves, the vacuum pumps were from SAES Getters, and a range of accessories including gaskets, bolts, blank flanges and tools were purchased from Kurt J Lesker, Vacom and LewVac. After the initial delay do to some of the components arriving late, the vacuum system was assembled in June 2018. This section outlines the procedures followed and issues encountered during the chamber assembly.

### 4.1.1 Preparation for the Assembly

In order to minimise the amount of dust present during assembly, the area around the optical table was isolated using plastic dust sheets. The inside of the isolated area was then wiped and dusted, along with all the tools and components to be used inside.

All vacuum components mounted on the setup were previously cleaned following the recommended procedures [24] [25] [26]. Metal parts were washed with acetone and rinsed with isopropanol. All components that could fit into the bath[1] were treated with ultrasound for 15 minutes in acetone, and then rinsed with isopropanol. Viewports were treated in a similar way, but with methanol rather than acetone, as it is less aggressive towards AR coatings. Immediately before mounting, flanges being connected and the gasket used were wiped with methanol using a lint free tissue.

### 4.1.2 Assembly

The first part of the system that was put together was the HV section, save for the effusion cell oven and the vacuum pumps to avoid exposing them to moisture for prolonged periods (they all arrived with flanged covers keeping them under vacuum), and viewports to protect the AR coatings from mechanical damage. The ZS mirror branch of the chamber was completed next, and after the compensation cage was positioned into place, the MOT chamber was connected to it. The remaining branches around the MOT chamber followed, with the ZS tube being the last part to be added, aligning the direction of the atomic beam in the process. Only after the passive chamber components were all assembled, the viewports, pumps and the oven were installed.

When the flanges were connected, the bolts were tightened using a star pattern. In order to assure uniform stress over the viewport flanges, fully annealed copper gaskets were used for viewports. Also, flanges were never tightened flush in order to allow some room for leak troubleshooting, if needed.

The oven was filled with 8.0 grams of erbium following the instructions from the manual. The erbium metal[2] was cut into small pieces, less than 3 *mm* in size, using clean wire cutters. The tantalum crucible of the oven was filled with erbium and assembled by fixing the apertures and the *hot lip* section in place The crucible was then carefully inserted into the body of the oven, watching out for the brittle ceramic discs holding the oven heaters, and then fixed in place using tantalum wire.

[1] Langford Sonomatic 375 ultrasound bath

[2] We purchased 25g of distilled dendritic erbium from Alfa Aesar

### 4.1.3 Vacuum Chamber Repair

In the very final stages of assembly, when the viewports on the MOT chamber were being installed, it was observed that some of the bolts holding the flanges are slipping inside the tapped holes. This prevented us from establishing good flange connections. After quickly examining the threads in the affected holes, it was observed they were visibly too shallow. Further inspection showed that the internal diameter of the tapped holes was between 5.5 *mm* and 5.7 *mm*, instead of 5.0 *mm* according to the M6 standard, for all the holes on the DN40CF flanges in the horizontal plane of the MOT chamber (Figure 4.1) - 24 holes in total! As the faulty behaviour of the threads was observed while finger-tightening the bolts, it is impossible that the threads were damaged by us. The cause was most probably a wrong diameter drill used by the manufacturer during machining. Following consultations with the student workshop supervisor at the Cavendish Laboratory, it was decided to attempt to refurbish the damaged threads using *Helicoil* spirals. The refurbishment procedure was the following:

- the damaged thread was removed by boring down the hole with a 6.1 *mm* drill. And the hole was chamfered at 45°, 1 *mm* deep.
- the widened hole was tapped with the special tapping tool provided in the *Helicoil* refurbishment set.
- the *Helicoil* spiral was inserted using the provided insertion tool and the guiding tip of the spiral was removed by knocking it off using a hammer and a metal rod.

### 4.1.4 Leak Checking and Pumpdown

Once the chamber was closed, a turbo-molecular pump was attached to one of the pumping ports. The turbo is backed by a scroll pump as it can only function at output pressures below 10 *mbar*. The leak checker, which is basically a mass spectrometer detecting helium[3], was attached to the output of the turbo pump. The flange connections were then leak tested by spraying helium around them and monitoring the leak rate on the detector. Wherever a leak was detected, additional tightening was tried first. If there was no result, the gasket was replaced and the pumpdown process was repeated. After all the leaks have been treated, the chamber was pumped down to $10^{-6}$ *mbar* with the turbo pump, making it ready for turning on the erbium oven.

[3]Leybold Œrlikon UL 200 Helium Leak Detector


Fig. 4.1 Measurement of the internal diameter of a tapped M6 bolt hole for the DN40CF flange showing the damage of the thread. The callipers are reading 5.65mm and while a healthy thread should have a 5.0mm internal diameter

## 4.2 Laser Systems

### 4.2.1 Blue Laser System

The blue laser system was installed in May 2017. The output power of the 401nm light was initially measured to be 2.1W, which gives a comfortable amount of extra power on top what we actually need. One issue with this laser system was immediately spotted, the frequency doubling module was very sensitive to vibrations and even a small hit to the optical table could unlock the laser and leave the power down for several seconds. Closer examination revealed that the piezo crystal used to stabilize the doubling cavity has resonances at approximately 2 $kHz$ (Figure 4.2). Also, it was observed that if the 'automatic relocking' procedure was disabled for the cavity, the intensity comes back much faster for all but very intensive disturbances. Although the system is fully functional in the absence of disturbances, concerns exist that installing shutters on the laser table may have detrimental

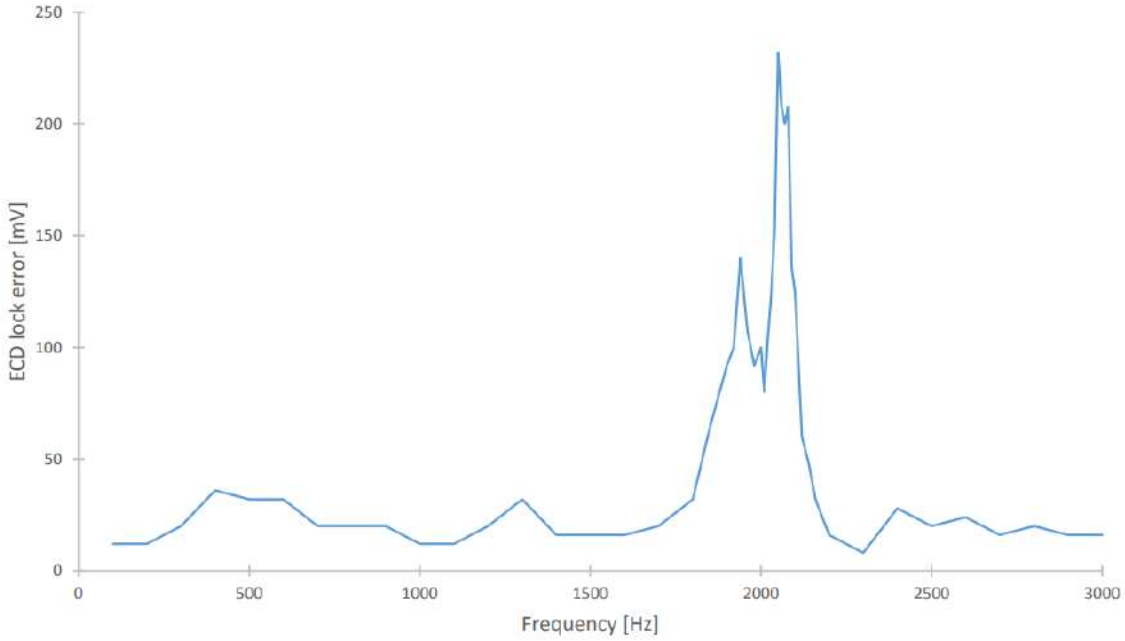


Fig. 4.2 The measured error signal of the blue laser doubling cavity feedback loop as a function of acoustic frequency. The acoustic perturbation was applied using a frequency generator and a loudspeaker

effect on the laser's behaviour. Therefore, we will design a circuit that will filter compensate for the piezo resonance by the means of a notch-filter[27].

The frequency locking scheme based on the Modulation Transfer Spectroscopy was implemented on the 401 *nm* laser system. Given the large natural linewidth of the blue transition in erbium, obtaining a sufficiently good lock was straightforward with the available hardware.

### 4.2.2 Yellow Laser System

Initially, it was intended to have separate spectroscopy systems for the two cooling lasers. Following the realisation that the second Hollow Cathode Lamp[4] that we have bought does not produce almost any erbium sputter, making it unusable for spectroscopy, the system was redesigned so that both lasers are locked using a single HCL. The diagram showing this system, implementing dichroic mirrors, was shown in the previous chapter (Figure 3.6).

In an attempt to measure the linewidth of the laser, a Delayed Self-Heterodyne Linewidth Measurement (DSHLM) setup was introduced at the pre-doubled output of the yellow laser -

[4]Supplied by Photron

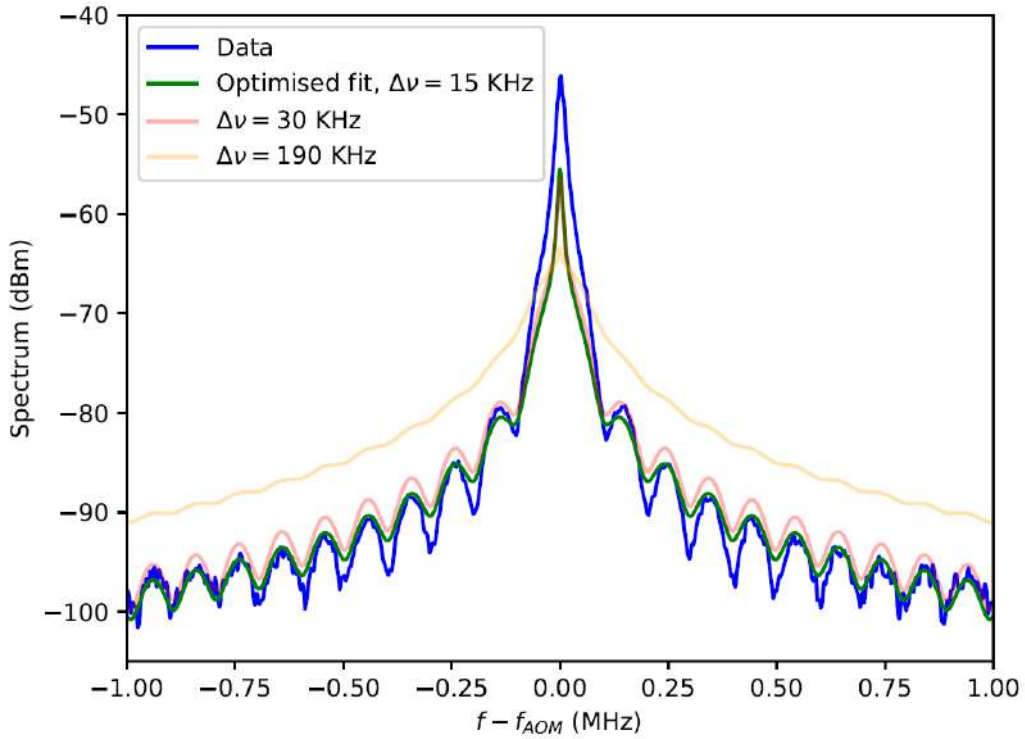


Fig. 4.3 The measured DSHLM signal and the theoretical fit (based on formalism from Appendix C), from [28]

with the 1166 *nm* light. The pre doubled light was chosen as the long, delay-fibre was easier and cheaper to get. In order to perform the measurement, the 1166nm output beam was demagnified with a telescope and then split into two components. One components was fed through an AOM at 80 $MHz$ while the other one was sent through 2km of optical fibre[5].

A Part III student performed the spectroscopy measurement using the described setup [28] and applying the formalism stated in Appendix C, he obtained the laser linewidth of 15kHz. Given the nature of the technique used, it is necessary to investigate this result further, as it rests on the assumption that the laser frequency has a white noise spectrum. If that does not hold, the measurement only confirmed that the short term linewidth over the timescales corresponding to the delay time of the fibre (i.e. $10\mu s$) is 15kHz, as the technique is decreasingly sensitive to noise components of lower and lower frequency.

### 4.2.3 Optical Transport System

A test setup was built on an optical table by a Part III student [19], to assess the feasibility of using the focus-tunable lenses for optical transport in our experiment. The aim was to

[5]Type OS2 communication fibre from FS.com

investigate whether we can create a high power trapping beam with a translatable focal point and variable waist size of reasonable quality and reproducibility, using a pair of these lenses, and given the degree of available optical access to the chamber. The introduction of a scanning AOM for further increasing waist size was also looked into. The conclusions were:

- it is possible to have a range of focus translation over the 30cm region required for optical transport in our experiment. The waist size can be independently set to any value from the interval between $25\mu m$ and $45\mu m$.
- it is necessary to mount the focus-tunable lenses horizontally, with the elastic surface facing upwards, to minimize the aberrations due to distortions of the membrane under gravity
- a scanning AOM can be successfully used to further increase the waist size of the trap up to $125\mu m$, aiming for better overlap with the MOT during atom transfer.
- with the optical powers in question, it might be necessary to apply a compensation circuitry feeding back (and/or forward) to the lens controller accounting for thermal drifts in the focal length

## 4.3 Electromagnet Coils

The Zeeman slower coil has been wound onto the vacuum tube before it was attached to the system. The tube was coled with blank flanges at both ends and additional support flanges with bored holes were attached from the outside. This allowed for the tube to be placed on a lathe for winding. The lathe was set to the lowest speed (50 rpm) and the wire was wound tight, layer by layer. Each layer was then glued with thermally conductive resin with thermal ratings compatible with the future baking process of the chamber. After the winding was completed, the full ZS coil was protected with kapton tape from the outside and the connections were checked for shorts.

The compensation cage coils were wound onto the appropriate frames and then the cage was assembled. For the 'y' and 'z' coils, for topological reasons, it was necessary to wind the wire prior to placing it into the frame - layer by layer, using a system of clamps and vices. After the coils were finished, they were checked for shorts, and any shorts found were treated with kapton tape.

# Chapter 5

# Outlook and Discussion

## 5.1 Future Plans and Timeline

Based on the progress made so far, we are aiming to finish all the basic building tasks by the end of 2018. The approximate timeline for setting up the apparatus is:

- 09 July 2018: Finish leak testing the chamber
- 14-16 July 2018: Turn on the erbium oven, and obtain an absorption signal before the Zeeman Slower
- 18 July 2018: Have all of the ZS and TC optics in place.
- 20 July 2018: Finish setting up computer control
- 22 July 2018: Set up all the MOT optics and coils + imaging
- end of July 2018: obtain a signal in the MOT and start optimizing ZS, TC and MOT parameters
- 06-10 August 2018: Lab moving to Oxford
- Mid September 2018 : The IR laser arrives, start setting up the transport stage
- Late September 2018: install science cell and reattach roughing pumps
- Early October 2018: Bakeout for 2 weeks
- Late October 2018: Obtain BEC through evaporative cooling
- End of 2018: install the SLM and create the optical box potential

In parallel with these milestones, numerous smaller tasks have to be completed in parallel in the immediate following period. This includes processing the atomic beam simulation results further to obtain insight into ZS parameter values, analysing the types of noise and the locking quality of the 583 *nm* to verify that the true obtained linewidth is indeed satisfactory, constructing miscellaneous electronics...

Having the atoms condensed and loaded into the optical box brings us to the point at which we can start with research work. There are several projects in plan, and here I describe the ones that are the first to be done. None of the projects are fully planned out yet so they are not in their ultimate form. Each of them will also require an additional set of tools to be installed onto the experimental setup.

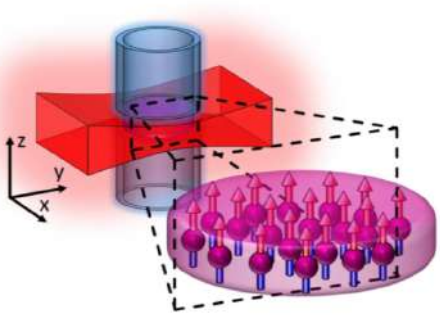


(a) Polarized gas of erbium atoms captured in a 2D box poential

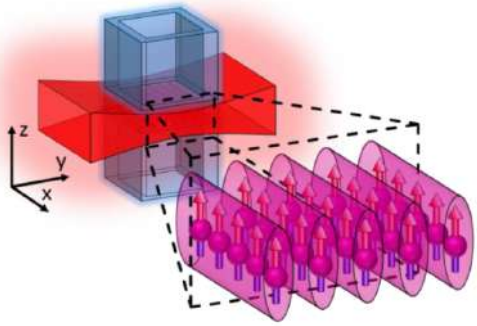


(b) A 1D array of tubes, the structure that might exhibit supersolid behaviour

### 5.1.1 Project 1 - Roton minimum

The first project we plan to perform upon setting up the optical box potential is to measure the excitation spectrum of a polarized quasi-2D gas in a configuration shown on Figure 5.1a. We expect to observe the softening of the Bogoliubov spectrum as the dipolar character of the gas is increased. This has already been observed for quasi-1D systems of dipolar quantum gases.

The explanation for such behaviour lies in the anisotropic nature of the dipole-dipole interaction. Since the force between two parallel dipoles is attractive (reduced potential energy) if they are collinear and repulsive (increased potential energy) if they are in the plane orthogonal to the dipole direction, any transversal perturbations present in a polarized quasi-2D gas of dipolar atoms will have an energy contribution originating from this term. Starting from zero wave number (no disturbance, flat 2D gas - maximally repulsive configuration) and increasing the wave number of the disturbance, neighbouring atoms are pushed more

and more towards the attractive configuration. Therefore, the DDI contribution to the energy decreases with wave number. As the regular Bogoliubov spectrum monotonously increases, for a sufficiently strong dipolar character of the gas, the spectrum might show a minimum at a finite wave vector - which is exactly the roton minimum. Quite expectedly, the energy will still go to increasing positive values at sufficiently high wave vector, as the kinetic energy term must eventually take over.

### 5.1.2 Project 2 - Supersolidity

Various models predict that a softened excitation spectrum exhibiting a roton minimum might enable the formation of a supersolid phase in a system of dipolar atoms. The supersolid is a phase that exhibits both superfluid flow and spatial order. It is predicted that a gas in a 2D lattice should show such behaviour, but the temperature scales at which it is due to happen are still out of reach in experiments. On the other hand, for a 1D array of tubes at high fillings, shown on Figure 5.1b, a supersolid is expected to arise at temperatures in the range of hundreds of nano kelvin neighbourhood.

### 5.1.3 Introducing the Second Species

At some point over the course of the experiment, the idea is to introduce an additional species, to investigate situations such as an impurity in a dipolar BEC. A good candidate for the second species is potassium, as it has an accessible Feshbach resonances, both bosonic and fermionic isotopes, and the techniques for cooling it are available. There is a valved off branch in the vacuum chamber that can house the 2D MOT for potassium, which can them be fed directly to the central MOT chamber. All of the MOT viewports have been coated such that the potassium MOT can be set up in parallel (at 767 *nm*).

The second species will allow us to test various models from the domain of condensed matter theory, but also quantum information. Implementation of various impurity and two species models realisable on lattices or uniform potentials will be within reach. Furthermore, addressing problems such as information loss in qubits[29] [30] is also the part of the plan.

## 5.2 Conclusion

We are building an experiment to investigate many-body physics in quantum systems with long-range, dipole-dipole interactions. The usage of the optical box potential should provide us with an enhanced insight to the intrinsic properties of these systems as the translational symmetry implies the absence of a length scale originating from the trap.

Continuing onto the work done so far, we should be able to set up laser cooling in the following weeks. Bose-Einstein condensation should be achieved by the late autumn this year in parallel with integrating the optical transport system onto the experiment. Setting up the optical box potential would follow immediately marking the start of research aimed project. At the beginning, an excitation spectrum of a quasi-2D gas of erbium atoms will be recorded for varying ratios of the s-wave and dipolar scattering lengths in the quest for a roton minimum. The next step would be a trial to realize a supersolid phase that is expect to arise in a 1D lattice of tubes as a consequence of such an excitation spectrum. Moving away from roton physics, we also plan to investigate the behaviour of driven and quenched system looking more closely into the terms of equilibrium and thermalisation. Furthermore, introducing a second atomic species will allow us to test more elaborate condensed matter models and touch on the subjects relevant to quantum information, such as decoherence and information loss suppression.

Over the course of my PhD, I plan to finish the full experimental setup and dwell onto the tasks regarding roton physics and driven and quenched systems. Depending on the degree of success and progress, the expansion of the vacuum chamber in order to add potassium might also be realized.

# Appendix A

# Computer Simulation of the Atomic Beam

In order to better understand the process of slowing down the atoms effusing from the oven, in order to load the MOT, I have written a computer simulation of the whole process in MATLAB. The simulation describes the beam from its creation in the effusion cell to the end of the path at the centre of the MOT, implementing transversal cooling and the Zeeman Slower along the way. The beam is represented in the simulation by a given number of atoms, with initial parameters generated from appropriate distribution functions, that are propagated through the system one-by one.

## A.1 Models for the simulation

### A.1.1 Effusion Cell

Erbium used in our experiment is dispensed from a high temperature oven. As shown in the figure, the oven consists of two chambers fitted with apertures. Solid erbium material is placed into the first chamber, the *effusion cell*, which is equipped with a set of heaters and is typically kept at temperatures between $1000\,\mathrm{deg}C$ and $1200\,\mathrm{deg}C$ during normal operation. At these temperatures the vapour pressure of erbium in the cell is significant, and atoms effuse through the tubular aperture into the second chamber of the oven - the *hot lip*. This part of the oven has separate heaters, and it's usually maintained at a slightly elevated temperature compared to the effusion cell, to avoid condensation of erbium on the second aperture, which is at the same time the output port of the oven.

The vapour pressure in the effusion cell can be estimated using the Antoine equation:

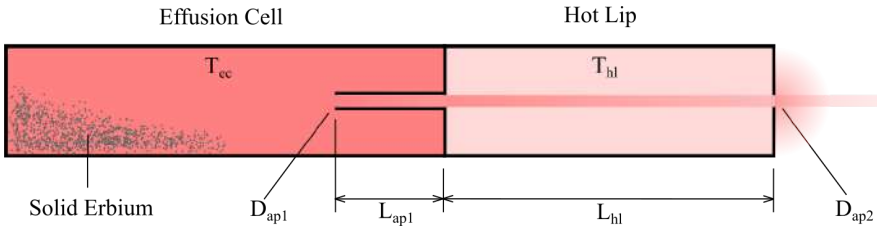


Fig. A.1 Drawing of the erbium oven chambers showing the effusion cell and the hot lip

$$p_{vap}(T) = 10^{A-\frac{B}{C+T}} \tag{A.1}$$

where the empirical constants for erbium are $A_{Er} = 7.103(4)$, $B_{Er} = 12170(20)$ and $C_{Er} = 100(2)$ for temperature expressed in degrees Celsius. The atoms from the erbium saturated cell effuse towards the hot lip section through a tubular aperture of diameter $D_1 = 3mm$ and length $L_1 = 30mm$. The distribution of the flux of the atoms at the entry to the circular aperture can be calcualted as:

$$\frac{d\Phi}{dvd\theta} = \left(\frac{m}{2\pi k_B T_{ec}}\right)^{\frac{3}{2}} 4\pi v^2 e^{-\frac{mv^2}{2k_B T_{ec}}} \frac{nv\sin\theta\cos\theta}{4\pi} \tag{A.2}$$

In the simulation, a representative sample of atoms that enter the tubular aperture is generated from the following distribution functions (employing a uniform random variable from the unit interval, *rand*):

$$v = \sqrt{-\frac{2k_B T_{ec}}{m}\left(1 + \mathcal{W}\left(\frac{rand-1}{e}\right)\right)} \tag{A.3}$$

$$\theta = \sin^{-1}\left(\sqrt{rand}\right) \tag{A.4}$$

$$\phi = 2\pi rand \tag{A.5}$$

and the spatial position where the atom enters the aperture is chosen randomly using a uniform distribution over the aperture. The atoms are then propagated along the tube, rethermalising them every time they hit the tube wall. The rethermalisation process implies assigning the atom with a new velocity generated from a Maxwell-Boltzmann distribution at temperature $T_{hl}$ and new direction of motion selected randomly. In order to check the

validity of this model, the proportion of the atoms that pass through the tube is compared with a known formula...

In order to normalize the results of the simulation later, the total rate of effusion into the tube is estimated by integrating the formula from above:

$$R_{ec} = \sqrt{\frac{\pi}{2k_B T_{ec} m}} P_v ap(T_{ec}) \frac{D_1^2}{4} \tag{A.6}$$

The atoms that make it through the first aperture are propagated further along the oven, through the hot lip section. The atoms that exit the oven through the second aperture are saved in a sample file, whereas the ones that hit the walls of the hot lip are rethermalised and then an appropriate proportion of them is added to the sample accounting for the atoms that effuse directly from the hot lip.

### A.1.2 Transversal Cooling

In the transversal cooling stage, two pairs of counter-propagating beams are directed onto the atomic beam from transversal directions. In the simulation, as the atoms travel through the chamber, in every time step, the intensities of all light fields are calculated at the current position of the atom, and the number of scattered photons from each of the beams is estimated. For high saturation parameters, the effects of the four fields on the atom cannot be viewed as independent. In order to model this complicated photon scattering scenario, the excited state is represented by four degenerate states, each coupled to the ground state by one of the light fields. An artificial 'decay' is introduced between the four excited states, to equalize their populations, but the effect on this term on the coherences involving the ground state is assumed not to exist. Solving the master equation gives the total excited state population, that is then used to calculate the total number of scattered photons in the time step. The fractions of absorbed photons between the four beams are assumed to be proportional to the scattering rates. The appropriate momentum adjustment, including the shot and spontaneous emission noise contributions, is then performed.

### A.1.3 Zeeman Slower

The Zeeman slower is treated in very much the same way as transversal cooling, only here the absorption rate can be directly calculated based on the light intensity and the effective detuning (that contains the actual laser detuning, along with the Doppler and Zeeman shifts). The magnetic field profile in the Zeeman slower is calculated prior to propagating atoms, using the Biot-Savart law.

## A.2 Simulation Results

The files containing representative samples of 500000 atoms effusing from the oven were generated for oven temperatures of 1000°C, 1050°C, 1100°C, 1150°C and 1200°C. In all cases, the hot lip temperature was kept at $T_{hl} = T_{ec} + 100°C$. The effusion rate and the expected lifetime of the erbium material that was loaded into the oven are shown on Figures A.2a and A.2b. The velocity distributions of the atomic beam coming out of the oven are plotted on the Figures A.3a and A.3b.

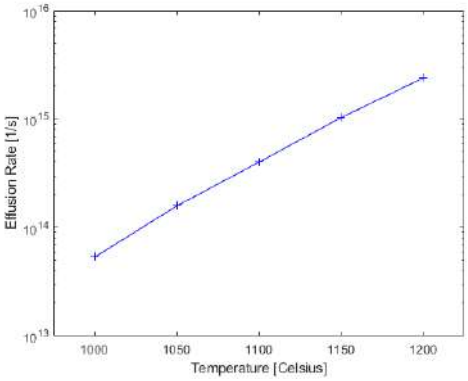


(a) Total rate of effusion from the erbium oven

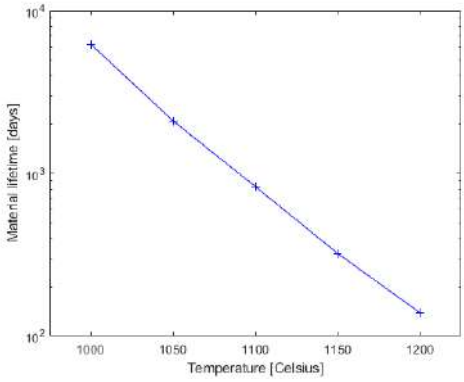


(b) The number of working hours for the oven at different temperatures, corresponding to 8 g of erbium material

Fig. A.2

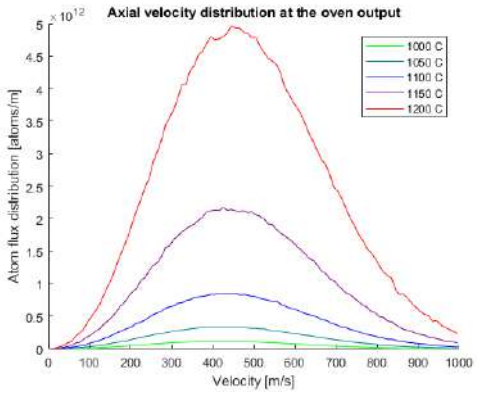


(a) Axial velocity distribution at the oven output for different temperatures

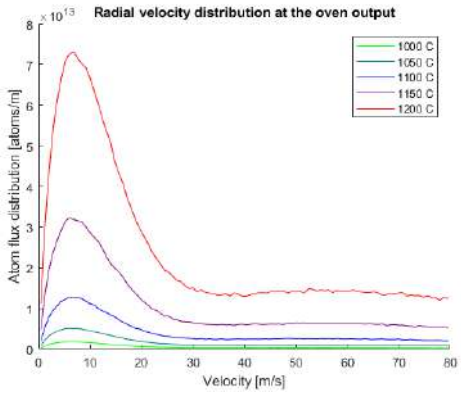


(b) Radial velocity distribution at the oven output for different temperatures

Fig. A.3

The atomic beam first encounters the external aperture that was fitted at the entrance to the TC cube. The fraction of atoms that are withheld by this aperture is measured to be

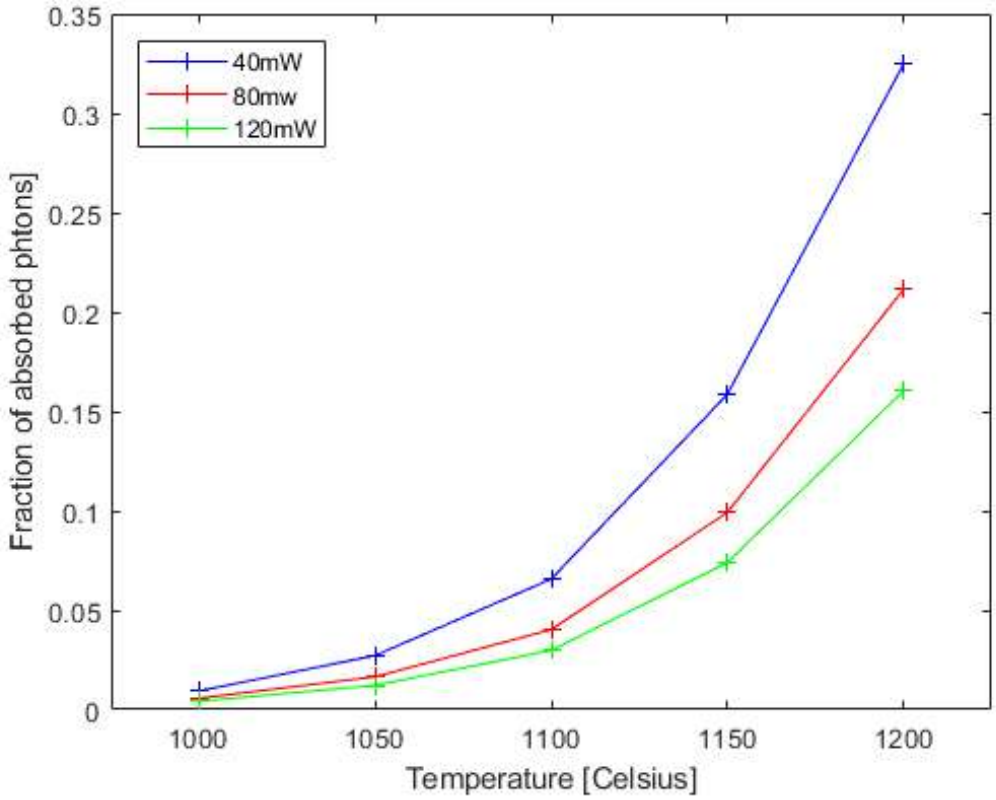


Fig. A.4 Fraction of absorbed photons from TC beams for different oven temperatures and laser powers. The TC beams in this simulation had waists $w_{TCx,y} = 4$mm and$w_{TCz} = 30$mm. The laser detuning was $\delta_{TC} = -10$MHz

0.9630 and is constant to within 0.1% variations, showing no clear trend with changing the temperature over the range used in the simulation. It is of paramount importance to prevent the excess atoms from reaching the TC stage, as the fractions of absorbed photons from the TC beams are already considerable for the non-divergent atoms as can be seen in Figure A.4.

The RMS waist of the atomic beam at the start of TC is measured to be 7.1mm along either of the directions. Mode-matching the TC laser beams with this waist is probably sub-optimal, as the atoms closer to the centre of the beam are more probable to actually go through the system, so cooling them preferentially should be a better approach. In order to obtain a more sensible value for $w_{TCx,y}$, the waist of the atomic beam is calculated at the start of TC including only the atoms that eventually reach the MOT chamber having the axial velocity smaller than the MOT capture velocity. In this case, the waist turns out to be 3.7mm. The spatial distribution in both cases is shown on Figure A.5. The waists quoted in both cases are $\frac{1}{e^2}$ waists obtained by fitting a gaussian.

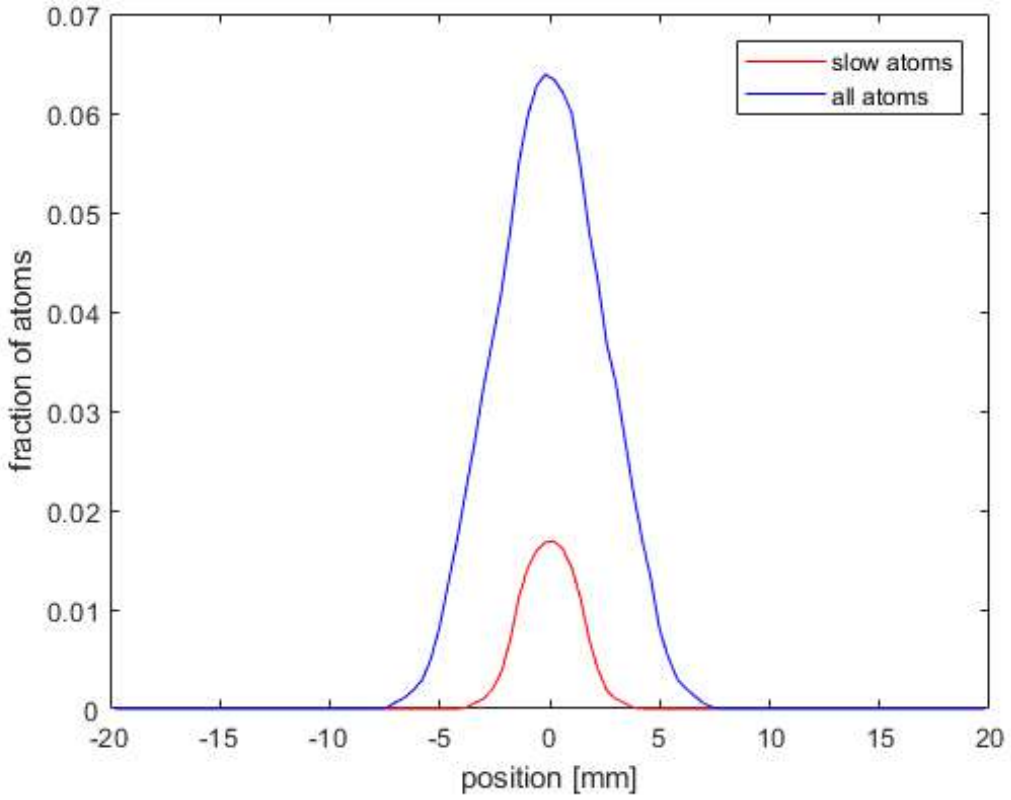


Fig. A.5 Fraction of absorbed photons from TC beams for different oven temperatures and laser powers. The TC beams in this simulation had waists $w_{TCx,y} = 4$mm and$w_{TCz} = 30$mm. The laser detuning was $\delta_{TC} = -10$MHz, the oven temperature is 1100°C

In the rest of the simulation $w_{TCx,y} = 3.7$mm is used. In order to see how the cooling efficiency depends on the waist along the axial direction, the rms velocity at the end of TC is recorded for different values of $w_{TCz}$ and the resluts are shown in Figure A.6.

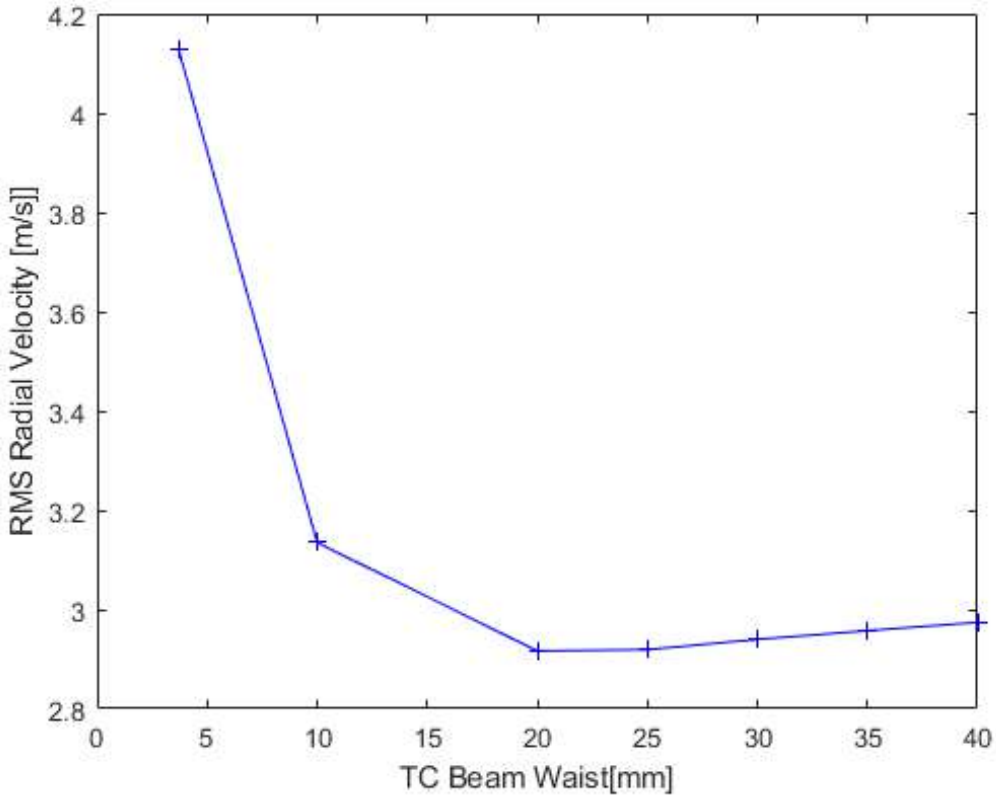


Fig. A.6 RMS velocity after TC for different axial waists

From this point we use $w_{TCz} = 30$mm which is slightly above the measured minimum, to ensure good performance for all parameter combinations, as the dependence on Figure A.6 is clearly flatter on the right of the minimum than on the left.

At the time of writing this report, the data and results from the atomic beam simulation haven't been processed past this point. This is among the tasks for the period immediately following the handing in of the report.

## A.3 Code

For increased clarity and compactness, the code presented here only contains the functional core, whereas all the parts related to plotting and output of the results were left out.

*SimulationOven.m*:

```
rng('shuffle');

N1=5000; %Trial sample size for determining probabilities
N2=500000; %Size of the generated output sample
Toven=1273;
Thl=Toven+100;
M_Er=166*1.67e-27;
Dap1=0.003;
Lap1=0.03;
Lhl=0.05;
Dap2=0.003;

thetamax=0.2; %maximum angle in radians generated in output

s1='w';
s2='fin';
Filename=['Atoms' s1 'Ap' num2str(Toven-273) s2 '.mat'];
K=0;
M2=0;
atoms = zeros(N2,5);

k_b=1.38e-23;
%Count the number of atoms passing through tube, and passing through second
%aperture
for n=1:N1
    [1 n]
    [vx,vy,vz,x,y] = Effusion_Out(Toven,M_Er,Dap1,pi/2);
    [pass,x,y,vx,vy,vz]=TubeDiff(Dap1,Lap1,Thl,M_Er,x,y,vx,vy,vz);
    if pass
        K=K+1;
        [x,y,vx,vy] = Propagate(x,y,Lhl,vx,vy,vz,3*pi/2);

        hit = CheckHit(x,y,Dap2);

        if hit
            M2=M2+1;
        end
    end

end

K=K/N1;
M=1-M2/(K*N1);
n=0;
n2=0;

Qec = sqrt(pi/(2*k_b*Toven*M_Er))*P_Vap(Toven)*Dap1^2/4;

Req=K*(1-M)/(1+K);
Qoutout=Qec*(Req+M*K);


%Generate sample
while n2<N2
    %effusion from effusion cell
```

```
    [vx,vy,vz,x,y] = Effusion_Out(Toven,M_Er,Dap1,pi/2);
    [pass,x,y,vx,vy,vz]=TubeDiff(Dap1,Lap1,Thl,M_Er,x,y,vx,vy,vz);
    if pass
        [x,y,vx,vy] = Propagate(x,y,Lhl,vx,vy,vz,pi/4);
        hit = CheckHit(x,y,Dap2);
        %if hits the hot lip, effuse out or back to effusion cell
        if hit && rand<=1/(1+K)

            hit=false;
            [vx,vy,vz,x,y] = Effusion_Out(Thl,M_Er,Dap2,pi/2);
        end

        if ~hit
            n=n+1;
            if atan(sqrt(vx^2+vy^2)/vz)<=thetamax
                n2=n2+1;
                %[2 n2]
                atoms(n2,:)=[vx,vy,vz,x,y];
            end
        end
    end
end

Qo1=Qoutout*n2/n; %atom flux contained within thetamax
Qd2=Qoutout-Qo1;  %atom flux discarded due to thetamax

AtomBeam = OvenAtoms(atoms,Toven,Thl,Dap1,Dap2,Lap1,0,Lhl,thetamax,Qo1,0,Qd2,K,M);
save(Filename,'AtomBeam');
```

*Loading_main.m*:

```
rng('shuffle');

%=========================================================================
% CONSTANTS:
M_au = 1.66e-27;                                        %Atomic unit mass
k_b = 1.38e-23;                                       %Boltzmann constant
h_bar = 6.62/2/pi*1e-34;                            %Reduced Planck constant
mu_b = 9.274e-24;                                             %Bohr Magneton
grav=9.81;                                         %Gravitational accelaration
phi_g = -3/2*pi;      %angle between g and the x axis (set to -y direction)


%-------------------------------------------------------------------------


%=========================================================================
% SIMULATION PARAMETERS

nisotope = 5;                                                 %Select isotope

atst1='AtomswAp'; %strings in the name of the atoms file [atst1 temp atst2]
atst2='fin.mat';

N_zs = 500;                %number of sampling steps for Zeeman slower field
N_tc = 500;               %number of iteration steps for transversal cooling
```

```
%-------------------------------------------------------------------------


%=========================================================================
% ERBIUM PROPERTIES
M_Er = Isotope * M_au;                              %Mass of one erbium atom
G_blue = 2*pi*29.7e6;              %Natural linewidth of the blue transtion
lambda_blue = 401e-9;                                %Blue light wavelength
k_blue = 2*pi/lambda_blue;                           %Blue light wavevector
Isat_blue = 0.06;                        %Blue saturation intensity (W/cm^2)
G_loss = 7.7e-6*G_blue;                            %Rate of dark state losses
vrec=h_bar*k_blue/M_Er;                                    %recoil velocity

Isotopes = [162 164 166 167 168 170];
Abundances = [0.0014 0.0161 0.336 0.23 0.268 0.15];

Isotope = Isotopes(nisotope);                      %Which Er isotope is used?
R_isotope=Abundances(nisotope);                            %Isotope abundance
%-------------------------------------------------------------------------


%=========================================================================
% OVEN PARAMETERS
Dap3 = 0.008;                                  %Radius of the third aperture
Lap3 = 0.053;                                 %Distance to the third aperture

Toven = 1100;      %Temperature of the Effusion Cell used in the simulation
%-------------------------------------------------------------------------


%=========================================================================
% TC STAGE PARAMETERS
Ltci = 0.0365;                         %Distance to the start of the TC stage
Ltc=0.035;                                          %Length of the TC stage
Ltcf = 0.0365;

P_tc= 0.08;                             %TC Beam power used in the simulation
Np=P_tc/h_bar/3e8/k_blue*4;   %Total number of available photons per second

TC_deltas = 10;                                                % TC detuning


wz_tc=0.03;                             %TC beam waist along axial direction
wxy_tc=0.004;                     %TC beam waist along transversal direction


dz_tc = Ltc/N_tc;                    %iteration step for transversal cooling
%-------------------------------------------------------------------------


%=========================================================================
% ZS STAGE PARAMETERS
Lzsi = 0.2585;                         %Distance to the start of the ZS stage
Dzs = 0.008;                                        %diameter of the ZS tube
```

```
Lzs=0.42;                                                %length of the ZS coils
Lzsf=0.158;                                          %Propagation distance after ZS

Izsbias=-3.55;                                         %Current in the bias coil
Izsprof=6.56;                                        %Current in the profile coil
Icomp1 = -2.146;                          %Current in the front compensation coil
Icomp2 = -0.245;                           %Current in the back compensation coil

P_zs = 0.08;                                                        %ZS beam power
w_zs1 = 0.005;                  %ZS beam waist at the end of the Zeeman Slower
w_zs2 = 0.005;                %ZS Beam waist at the start of the Zeeman Slower

theta_zs = atan((w_zs1-w_zs2)/(2*Lzs));%focusing angle of the ZS laser beam
Lf_zs = w_zs2/2/tan(theta_zs);

mu_prime=mu_b*muprime(-7,-6);              %magnetic moment of the transition

deltazs=-2*pi*490e6;                                      %ZS light detuning


dz_zs = (Lzs+Lzsi+Lzsf)/N_zs;                      %sampling step for ZS field

%ZS B-field sampling
Bzs=zeros(N_zs,1);
for nzs = 1:N_zs+1
    z=-Lzsi+nzs*dz_zs;
    Bzs(nzs)=zsfield(z,Izsbias,Izsprof,Icomp1,Icomp2)/10000;
end
%--------------------------------------------------------------------------


load([atst1 num2str(Toven) atst2]);
load(['TCGrid' num2str(TC_deltas*10) '.mat']);
atoms=AtomBeam.Atoms;
N_atoms=size(atoms,1);



%Monte-Carlo Loop
for nsim=1:N_atoms

    hit = false;

    vx=atoms(nsim,1);
    vy=atoms(nsim,2);
    vz=atoms(nsim,3);
    x=atoms(nsim,4);
    y=atoms(nsim,5);

    %Propagate to the third aperture and check if it hits
    if ~hit
        [x,y,vx,vy] = Propagate(x,y,Lap3,vx,vy,vz,phi_g);
        hit = CheckHit(x,y,Dap3);
    end

```

```
136     %propagate to the TC stage
137     if ~hit
138         [x,y,vx,vy] = Propagate(x,y,Ltci,vx,vy,vz,phi_g);
139     end
140
141     Nsc=0;
142     Nsci=0;
143     %transversal coolings
144     if ~hit
145
146         if ~P_tc==0
147             for ntc = 1:N_tc
148                 z=ntc*dz_tc;
149                 %calculate intensities in the two beams
150                 Itcx=P_tc(ni)*2/pi/wz_tc/wxy_tc*exp(-2*(y^2/wxy_tc^2+(z-Ltc*0.5)^2/
    wz_tc^2))/10000;
151                 Itcy=P_tc(ni)*2/pi/wz_tc/wxy_tc*exp(-2*(x^2/wxy_tc^2+(z-Ltc*0.5)^2/
    wz_tc^2))/10000;
152                 %extract the appropriate exc. state population from the grid
153                 n1=round(limitval(sqrt(Itcx/TCpar(1)))*(TCgs(1)-1))+1;
154                 n2=round(limitval(sqrt(Itcy/TCpar(2)))*(TCgs(2)-1))+1;
155                 n3=round(limitval((abs(vx))/TCpar(3))*(TCgs(3)-1))+1;
156                 n4=round(limitval((abs(vy))/TCpar(4))*(TCgs(4)-1))+1;
157                 TCP=TCpop(n1,n2,n3,n4);
158                 %change the velocities to account for scattering
159                 Nsc=Nsc + TCP*G_blue*dz_tc/vz;
160                 [dvx,dvy]=TCForce(TCP,vx,vy,k_blue,delta_tc,G_blue,dz_tc/vz,M_Er);
161                 vx=vx+dvx;
162                 vy=vy+dvy;
163                 %propagate atom in this time step
164                 [x,y,vx,vy] = Propagate(x,y,dz_tc,vx,vy,vz,phi_g);
165             end
166         else
167             [x,y,vx,vy] = Propagate(x,y,Ltc,vx,vy,vz,phi_g);
168         end
169
170         %count the absorbed photons
171         Nsci=Nsci+Nsc*AtomBeam.RateOut/N_atoms*R_isotope;
172     end
173
174     %Propagate to the start of the ZS and check if it hits
175     if ~hit
176         [x,y,vx,vy] = Propagate(x,y,Ltcf,vx,vy,vz,phi_g);
177         hit = CheckHit(x,y,Dzs);
178     end
179
180     %Zeeman Slowing
181     if ~hit
182         z=0;
183         vz0=vz;
184         while z<Lzsi+Lzs && vz>0 && ~hit
185
186             z=z+vz/vz0*dz_zs;
187             w_zs = w_zs1+(z-Lzsi)/Lzs*(w_zs2-w_zs1);
188             B=B_sampled(Bzs,z,Lzsi+Lzs+Lzsf);
```

```
189             S_zs = P_zs*2/pi/w_zs^2*exp(-2*(x^2+y^2)/w_zs^2)/Isat_blue/10000;
190             %calculate the direction of the photons
191             theta1_zs = atan(sqrt(x^2+y^2)/(z+Lf_zs-Lzsi));
192             if x>=0
193                 phi1_zs = atan(y/x);
194             else
195                 phi1_zs = pi-atan(-y/x);
196             end
197             %change velocities to account for scattering
198             Fzs=F_scatt(vz*cos(theta1_zs)+vy*sin(theta1_zs)*sin(phi1_zs)+vx*sin(
    theta1_zs)*cos(phi1_zs),k_blue,S_zs,deltazs-B*mu_prime/h_bar,G_blue);
199             dt_zs=dz_zs/vz0;
200             vz=vz+cos(theta1_zs)*Fzs/M_Er*dt_zs+vrec*sign(rand-0.5)*sqrt((abs(cos(
    theta1_zs))+1/3)*abs(Fzs)/M_Er/vrec*dt_zs);
201             vy=vy+sin(theta1_zs)*sin(phi1_zs)*Fzs/M_Er*dt_zs+vrec*sign(rand-0.5)*sqrt
    ((abs(sin(theta1_zs)*sin(phi1_zs))+1/3)*abs(Fzs)/M_Er/vrec*dt_zs);
202             vx=vx+sin(theta1_zs)*cos(phi1_zs)*Fzs/M_Er*dt_zs+vrec*sign(rand-0.5)*sqrt
    ((abs(sin(theta1_zs)*cos(phi1_zs))+1/3)*abs(Fzs)/M_Er/vrec*dt_zs);
203
204             if vz<=0
205                 hit = true;
206             end
207             [x,y,vx,vy]=Propagate(x,y,dz_zs,vx,vy,vz0,phi_g);
208         end
209
210         if ~hit
211             hit=CheckHit(x,y,Dzs);
212         end
213
214         while z<Lzsi+Lzs+Lzsf && vz>0 && ~hit
215
216             z=z+vz/vz0*dz_zs;
217             w_zs = w_zs1+(z-Lzsi)/Lzs*(w_zs2-w_zs1);
218             B=B_sampled(Bzs,z,Lzsi+Lzs+Lzsf);
219             S_zs = P_zs*2/pi/w_zs^2*exp(-2*(x^2+y^2)/w_zs^2)/Isat_blue/10000;
220             %calculate the direction of the photons
221             theta1_zs = atan(sqrt(x^2+y^2)/(z+Lf_zs-Lzsi));
222             if x>=0
223                 phi1_zs = atan(y/x);
224             else
225                 phi1_zs = pi-atan(-y/x);
226             end
227             %change velocities to account for scattering
228             Fzs=F_scatt(vz*cos(theta1_zs)+vy*sin(theta1_zs)*sin(phi1_zs)+vx*sin(
    theta1_zs)*cos(phi1_zs),k_blue,S_zs,deltazs-B*mu_prime/h_bar,G_blue);
229             dt_zs=dz_zs/vz0;
230             vz=vz+cos(theta1_zs)*Fzs/M_Er*dt_zs+vrec*sign(rand-0.5)*sqrt((abs(cos(
    theta1_zs))+1/3)*abs(Fzs)/M_Er/vrec*dt_zs);
231             vy=vy+sin(theta1_zs)*sin(phi1_zs)*Fzs/M_Er*dt_zs+vrec*sign(rand-0.5)*sqrt
    ((abs(sin(theta1_zs)*sin(phi1_zs))+1/3)*abs(Fzs)/M_Er/vrec*dt_zs);
232             vx=vx+sin(theta1_zs)*cos(phi1_zs)*Fzs/M_Er*dt_zs+vrec*sign(rand-0.5)*sqrt
    ((abs(sin(theta1_zs)*cos(phi1_zs))+1/3)*abs(Fzs)/M_Er/vrec*dt_zs);
233             if vz<=0
234                 hit = true;
235             end
```

```
            [x,y,vx,vy]=Propagate(x,y,dz_zs,vx,vy,vz0,phi_g);
        end

    end

    %count in the losses due to decay into dark state
    if ~hit

        ploss=1-exp(-G_loss/G_blue*(vz0-vz)/(h_bar*k_blue/M_Er));
        if rand<ploss
            hit=true;
        end

    end

end
```

*Effusion_Out.m*:

```
function [vx,vy,vz,x,y] = Effusion_Out(T,m,D,thmax)
    kb=1.38e-23;

    v=sqrt(-2*kb*T/m*(1+lambertw(-1,(rand-1)/exp(1))));
    thetav=asin(sqrt(rand)*sin(thmax));
    phiv=2*pi*rand;

    vz=v*cos(thetav);
    vr=v*sin(thetav);
    vx=vr*cos(phiv);
    vy=vr*sin(phiv);

    phi=rand*2*pi;
    r=sqrt(rand)*D/2;
    x=r*cos(phi);
    y=r*sin(phi);
end
```

*B_sampled.m*:

```
function B = B_sampled(Bzs,z,L)

N_zs=length(Bzs)-1;

nzlow=floor(N_zs*z/L+0.0000001);
nzres=N_zs*z/L-nzlow;
if (nzlow>0) || (nzlow>N_zs)
    B=Bzs(nzlow)*(1-nzres)+Bzs(nzlow+1)*nzres;
else
    B=0;
end

end
```

*BLoop.m*:

```
function[fieldout] = BLoop(z,zloop,Iloop,rloop)
%outputs the magnetic field, in Gauss, of a single current loop along the z
```

```
%axis

mu0 = 4*pi*10^-7;
fieldout = 10^4*(mu0*Iloop*rloop^2)/(2*((z-zloop)^2+rloop^2)^(3/2));

end
```

*CheckHit.m*:

```
function hit = CheckHit(x,y,D)

if x^2+y^2>D^2/4
    hit = true;
else
    hit= false;
end

end
```

*clebschgordan.m* NEED THE REFERENCE!!!:

```
function cg=clebschgordan(j1,j2,m1,m2,J,M)

% cg=clebschgordan(j1,j2,m1,m2,J,M)
%
% Calculates CG coefficient <j1j2m1m2|JM> for the angular momentum state
% providing the following are true:
%
% A: All m quantum numbers are projections of respective j value
%      |mi|<=ji
% B: Triangle relation satisfied:
%      |j1-j2|<=J<=j1+j2
% C: CG=0 unless m1+m2=M
%
% ClebschGordan coefficient evaluated using equation found in 'Angular
% Momentum: An Illustrated guide to Rotational Symmetries for
% Physical Systems', W. J. Thompson
%
%Special cases are entered manually to reduce computation
%
%J. Pritchard Durham University 2009

%Check Projections
if((abs(m1)>j1)||(abs(m2)>j2))
    disp(sprintf('j1:%1.2f,mj1:%1.2f,j2:%1.2f,mj2:%1.2f',j1,m1,j2,m2));
    error(sprintf('Values of m must satisfy projections onto j such that |m|<=j'));
%Check Triangular relation
elseif(((J<abs(j1-j2))||(J>(j1+j2))))
    error(sprintf('Addition of angular momentum requires triangle relation\n\t|j1-j2
    |<=J<=j1+j2'));
%Evaluate CG
else
    if(m1+m2~=M)
        cg=0;
    elseif(j2==0)
        cg=1;
```

```
    elseif(J==0)
        cg=(-1)^(j1-m1)/sqrt(2*j1+1);
    else
        cg=sqrt(2*J+1)*...
            exp(0.5*(lgf(J+j1-j2)+lgf(J-j1+j2)+lgf(j1+j2-J)+lgf(J+M)+lgf(J-M)...
            -lgf(j1+j2+J+1)-lgf(j1-m1)-lgf(j1+m1)-lgf(j2-m2)-lgf(j2+m2)))...
            *ksum(j1,m1,j2,m2,J,M);
    end
end

%Summation performed for all values of k which give non-negative factorials
function Ck=ksum(j1,m1,j2,m2,J,M)
Ck=0;
kmin=max([m1-j1,0,-j1+j2+M]);
kmax=min([J-j1+j2,J+M,j2+m1+J]);
for(k=kmin:kmax)
    Ck =Ck+(-1)^(k+j2+m2)*exp(lgf(j2+J+m1-k)+lgf(j1-m1+k)...
        -lgf(k)-lgf(J-j1+j2-k)-lgf(J+M-k)-lgf(k+j1-j2-M));
end

%Stirlings approximation ln(n!) = nln(n)-n+0.5ln(2pin)
function y=lgf(x)
if(x<170)
    y=log(factorial(x));
else
    y=x*log(x)-x+0.5*log(2*pi*x)+1/(12*x)-1/(360*x^3)+1/(1260*x^5)...
        -1/(1680*x^7)+1/(1188*x^9);
end
```

*F_scatt.m*:

```
function F=F_scatt(v,k,s,del,G)

h=6.62/pi/2*1e-34;

F=-h*k*G/2*s*1./(1+s+4*(del+k*v).^2/G^2);

end
```

*limitval.m*:

```
function b=limitval(a)

b=a;
b(b>1)=1;
b(b<0)=0;

end
```

*MB_dist.m*:

```
%this function calculates the Maxwell Boltzmann distribution
function f=MB_dist(v,T,m)

f=(m/(2*pi*1.38e-23*T))^1.5*4*pi*v^2*exp(-m*v^2/(2*1.38e-23*T));

end
```

*muprime.m*:

```
function m=muprime(me,mg)

ge=1.160;
gg=1.1638;

m=me*ge-mg*gg;

end
```

*nlw.m*:

```
function p=nlw(delta,G)

p=1./(1+4.*delta.^2/G^2);

end
```

*P_Vap.m*:

```
%This function calculates the vapur pressure of Erbium at a given
%temperature according to the Antoine equation. p is in Pa, T is in K.

function p = P_Vap(T)
A_Er = 7.103;
B_Er = 12170;
C_Er = 100;
p = 10^(2+A_Er-B_Er/(C_Er+T-273.15));
end
```

*Propagate.m*:

```
function [x_new,y_new,vx_new,vy_new]=Propagate(x_old,y_old,L,vx_old,vy_old,vz,pg)
grav=9.81;

vx_new=vx_old+grav/vz*L*cos(pg);
vy_new=vy_old+grav/vz*L*sin(pg);


x_new=x_old+(vx_old+vx_new)/vz*L/2;
y_new=y_old+(vy_old+vy_new)/vz*L/2;

end
```

*R_molasses.m*:

```
function R=R_molasses(v,k,s,del,G)

R=G/2*s*(1./(1+s+4*(del-k*v).^2/G^2)+1./(1+s+4*(del+k*v).^2/G^2));

end
```

*Rho22.m*:

```
function r=Rho22(O,delta,G,v,s)
k=2*pi/(401e-9);
r=0.25*O^2./((delta+k.*v).^2+s.*O^2/2+G^2/4);
```

```

end
```

*SimulationTC.m*:

```
delta0 = -2*pi*10e6;
Imax = 0.2;
vmax = 50;

Pop=TCRateEq2(Imax,Imax,vmax,vmax,75,75,delta0);

Grid = PopulationGrid(Pop,[Imax,Imax,vmax,vmax],delta0,[0,0]);

save('TCGrid100.mat','Grid');
```

*TCForce.m*:

```
function [dvx,dvy] = TCForce(pop,vx,vy,k,delta,G,dt,m)
h_bar = 6.62/2/pi*1e-34;
p0=nlw(delta+k*vx,G)+nlw(delta-k*vx,G)+nlw(delta+k*vy,G)+nlw(delta-k*vy,G);
p1=nlw(delta+k*vx,G)/p0;
p2=nlw(delta-k*vx,G)/p0;
p3=nlw(delta+k*vy,G)/p0;
p4=nlw(delta-k*vy,G)/p0;

vr=h_bar*k/m;

dvx = -h_bar*k*G*pop*(p1-p2)/m*dt+sign(rand-0.5)*vr*sqrt(pop*G*dt*(p1+p2+1/3));
dvy = -h_bar*k*G*pop*(p3-p4)/m*dt+sign(rand-0.5)*vr*sqrt(pop*G*dt*(p3+p4+1/3));

end
```

*TCnewmod.m*:

```
function dm = TCnewmod(ox,oy,d,kvx,kvy,g,g1,g2)

b=[0;0;0;0;0;-ox/2;0;-ox/2;0;-oy/2;0;-oy/2;0;0;0;0;0;0;0;0;0;0;0;0];
%  c1          c2          c3          c4          u1             v1             u2
     v2             u3             v3             u4             v4             u5          v5
           u6          v6             u7          v7              u8            v8
      u9            v9             u10         v10
M=[-(g+3*g2), g2,         g2,         g2,         0,             ox,            0,
     0,            0,             0,             0,             0,             0,          0,
           0,          0,             0,          0,              0,            0,
      0,           0,             0,          0;      ...     %c1
   g2,         -(g+3*g2), g2,         g2,         0,             0,             0,
     ox,           0,             0,             0,             0,             0,          0,
           0,          0,             0,          0,              0,            0,
      0,           0,             0,          0;      ...     %c2
   g2,         g2,         -(g+3*g2), g2,         0,             0,             0,
     0,            0,             oy,            0,             0,             0,          0,
           0,          0,             0,          0,              0,            0,
      0,           0,             0,          0;      ...     %c3
   g2,         g2,         g2,         -(g+3*g2), 0,             0,             0,
     0,            0,             0,             0,             oy,            0,          0,
           0,          0,             0,          0,              0,            0,
      0,           0,             0,          0;      ...     %c4
```

```
9   0,          0,          0,          0,          -(g+3*g1)/2, d+kvx,       0,
      0,          0,          0,          0,          0,          0,          -ox
     /2,     0,          -oy/2,         0,          -oy/2,         0,          0,
        0,          0,          0,          0;      ...     %u1
10  -ox,        -ox/2,      -ox/2,      -ox/2,      -(d+kvx),     -(g+3*g1)/2, 0,
      0,          0,          0,          0,          0,          -ox/2,      0,
           -oy/2,      0,          -oy/2,      0,          0,          0,
        0,          0,          0,          0;      ...     %v1
11  0,          0,          0,          0,          0,          0,          -(g+3*g1)/2,
      d-kvx,      0,          0,          0,          0,          0,          ox
     /2,     0,          0,          0,          0,          0,          -oy/2,
         0,          -oy/2,         0,          0;      ...     %u2
12  -ox/2,      -ox,        -ox/2,      -ox/2,      0,          0,          -(d-kvx),
      -(g+3*g1)/2, 0,          0,          0,          0,          -ox/2,      0,
           0,          0,          0,          0,          -oy/2,      0,
        -oy/2,      0,          0,          0;      ...     %v2
13  0,          0,          0,          0,          0,          0,          0,
      0,          -(g+3*g1)/2, d+kvy,      0,          0,          0,          0,
           0,          ox/2,       0,          0,          0,          ox/2,
        0,          0,          0,          -oy/2; ...      %u3
14  -oy/2,      -oy/2,      -oy,        -oy/2,      0,          0,          0,
      0,          -(d+kvy),     -(g+3*g1)/2, 0,          0,          0,          0,
           -ox/2,      0,          0,          0,          -ox/2,      0,
        0,          0,          -oy/2       0;      ...     %v3
15  0,          0,          0,          0,          0,          0,          0,
      0,          0,          0,          -(g+3*g1)/2, d-kvy,      0,          0,
           0,          0,          0,          ox/2,       0,          0,
        0,          ox/2,       0,          oy/2;   ...     %u4
16  -oy/2,      -oy/2,      -oy/2,      -oy,        0,          0,          0,
      0,          0,          0,          -(d-kvy)      -(g+3*g1)/2, 0,          0,
           0,          0,          -ox/2,      0,          0,          0,
        -ox/2,      0,          -oy/2       0;      ...     %v4
17  0,          0,          0,          0,          0,          ox/2,       0,
      -ox/2,      0,          0,          0,          0,          -(g+3*g2), -d,
           0,          0,          0,          0,          0,          0,
        0,          0,          0,          0;      ...     %u5
18  0,          0,          0,          0,          ox/2,       0,          -ox/2,
      0,          0,          0,          0,          0,          2*kvx,      -(g
     +3*g2), 0,          0,          0,          0,          0,          0,
        0,          0,          0,          0;      ...     %v5
19  0,          0,          0,          0,          0,          oy/2,       0,
      0,          0,          -ox/2,      0,          0,          0,          0,
           -(g+3*g2), -d-(kvx+kvy), 0,          0,          0,          0,
        0,          0,          0,          0;      ...     %u6
20  0,          0,          0,          0,          oy/2,       0,          0,
      0,          -ox/2,      0,          0,          0,          0,          0,
           kvx-kvy,    -(g+3*g2),     0,          0,          0,          0,
        0,          0,          0,          0;      ...     %v6
21  0,          0,          0,          0,          0,          oy/2,       0,
      0,          0,          0,          0,          -ox/2,      0,          0,
           0,          0,          -(g+3*g2), -d-(kvx-kvy), 0,          0,
        0,          0,          0,          0;      ...     %u7
22  0,          0,          0,          0,          oy/2,       0,          0,
      0,          0,          0,          -ox/2,      0,          0,          0,
```

```
           0,          0,             kvx+kvy,    -(g+3*g2),     0,           0,
      0,          0,             0,          0;      ...     %v7
   0,          0,          0,          0,          0,             0,           0,
     -oy/2,        0,             ox/2,         0,             0,           0,          0,
           0,          0,             0,          0,             -(g+3*g2),   -d-(kvx-kvy)
    , 0,          0,             0,          0;      ...     %u8
   0,          0,          0,          0,          0,             0,           oy/2,
     0,            -ox/2,        0,             0,             0,           0,          0,
           0,          0,             0,          0,             kvy-kvx,     -(g+3*g2),
      0,          0,             0,          0;      ...     %v8
   0,          0,          0,          0,          0,             0,           0,
     -oy/2,        0,             0,             0,             ox/2,        0,          0,
           0,          0,             0,          0,             0,           0,
      -(g+3*g2),   -d-(kvx+kvy),  0,          0;      ...     %u9
   0,          0,          0,          0,          0,             0,           oy/2,
     0,          0,             0,             -ox/2,         0,           0,          0,
           0,          0,             0,          0,             0,           0,
      -(kvx+kvy), -(g+3*g2),     0,          0;      ...     %v9
   0,          0,          0,          0,          0,             0,           0,
     0,          0,             -oy/2,         0,             oy/2,        0,          0,
           0,          0,             0,          0,             0,           0,
      0,          0,             -(g+3*g2),  -d;     ...     %u10
   0,          0,          0,          0,          0,             0,           0,
     0,          oy/2,          0,             -oy/2,         0,           0,          0,
           0,          0,             0,          0,             0,           0,
      0,          0,             2*kvy,      -(g+3*g2)];    %v10


a=M\b;
dm=sum(a(1:4));
end
```

*TCRateEq2.m*:

```
function tcr = TCRateEq2(Ixmax,Iymax,vxmax,vymax,NIsample,NVsample,delta0)

tcr = zeros(NIsample,NIsample,NVsample,NVsample);

% Naverage = 10;

G_blue = 2*pi*29.7e6;
Isat_blue = 0.06;
k_blue = 6.28/401e-9;


N=NVsample^2*NIsample^2;

for nix = 1:NIsample
    for niy = 1:NIsample
        for nvx = 1:NVsample
            for nvy = 1:NVsample

                percent=100*(nvy-1+NVsample*(nvx-1+NVsample*(niy-1+NIsample*(nix-1)))
    )/N

                if NIsample >1
```

```
                    Ix=(nix-1)/(NIsample-1)*Ixmax;
                    Iy=(niy-1)/(NIsample-1)*Iymax;
                else
                    Ix=Ixmax;
                    Iy=Iymax;

                end
                Ox = sqrt(0.5*Ix/Isat_blue);
                Oy = sqrt(0.5*Iy/Isat_blue);

                vx=(nvx-1)/(NVsample-1)*vxmax;
                vy=(nvy-1)/(NVsample-1)*vymax;


                tcr(nix,niy,nvx,nvy) = TCnewmod(Ox,Oy,delta0/G_blue,vx*k_blue/G_blue,
    vy*k_blue/G_blue,1,0,100);
            end
        end
    end
end

end
```

*TubeDiff.m*:

```
%Changed gravity direction to -y
function [pass,x1,y1,vx1,vy1,vz1]=TubeDiff(D,L,T,m,x,y,vx,vy,vz)
kb=1.38e-23;
out=false;
z=0;
% figure(1);
% hold on
% [X,Y,Z]=cylinder();
% X=D/2*X;
% Y=D/2*Y;
% Z=L*Z;
% surf(X,Y,Z,'FaceAlpha',0.2);
while ~out
    if vz>0
        [x1,y1,vx1,vy1]=Propagate(x,y,L-z,vx,vy,vz,3*pi/2);
        hit = CheckHit(x1,y1,D);
        if ~hit
            out=true;
            pass=true;
%             line([x,x1],[y,y1],[z,L]);
        end
        if hit
            z0=z;
            x0=x;
            y0=y;
            z=z0+vz*(vx*x0+vy*y0)/(vx^2+vy^2)*(sign(vx*x0+vy*y0)*sqrt(1+(vx^2+vy^2)*(
    D^2/4-x0^2-y0^2)/(vx*x0+vy*y0)^2)-1);
            x=x0+vx/vz*(z-z0);
            y=y0+vy/vz*(z-z0);
            vx=normrnd(0,sqrt(kb*T/m));
            vy=normrnd(0,sqrt(kb*T/m));
```

```
31              vz=normrnd(0,sqrt(kb*T/m));
32              if (vx*x+vy*y)>0
33                  vx=-vx;
34                  vy=-vy;
35              end
36 %              line([x0,x],[y0,y],[z0,z]);
37          end
38      end
39      if vz<0
40          [x1,y1,vx1,vy1]=Propagate(x,y,z,vx,vy,-vz,3*pi/2);
41          hit = CheckHit(x1,y1,D);
42          if ~hit
43              out=true;
44              pass=false;
45 %              line([x,x1],[y,y1],[z,0]);
46          end
47          if hit
48              z0=z;
49              x0=x;
50              y0=y;
51              z=z0+vz*(vx*x0+vy*y0)/(vx^2+vy^2)*(sign(vx*x0+vy*y0)*sqrt(1+(vx^2+vy^2)*(
    D^2/4-x0^2-y0^2)/(vx*x0+vy*y0)^2)-1);
52              x=x0+vx/vz*(z-z0);
53              y=y0+vy/vz*(z-z0);
54              vx=normrnd(0,sqrt(kb*T/m));
55              vy=normrnd(0,sqrt(kb*T/m));
56              vz=normrnd(0,sqrt(kb*T/m));
57              if (vx*x+vy*y)>0
58                  vx=-vx;
59                  vy=-vy;
60              end
61 %              line([x0,x],[y0,y],[z0,z]);
62          end
63      end
64      if vz==0
65          if ~vx==0
66              x0=x;
67              y0=y;
68              x=x0-((vx*x0+vy*y0)/vx-sqrt(D^2/4*(1+vy^2/vx^2)-(y0-vy/vx*x)^2))/(1+vy^2/
    vx^2);
69              y=y0+vy/vx(x-x0);
70          end
71          if ~vy==0
72              y0=y;
73              x0=x;
74              y=y0-((vy*y0+vx*x0)/vy-sqrt(D^2/4*(1+vx^2/vy^2)-(x0-vx/vy*y0)^2))/(1+vx
    ^2/vy^2);
75              x=x0+vx/vy(y-y0);
76          end
77          vx=normrnd(0,sqrt(kb*T/m));
78          vy=normrnd(0,sqrt(kb*T/m));
79          vz=normrnd(0,sqrt(kb*T/m));
80          if (vx*x+vy*y)>0
81              vx=-vx;
82              vy=-vy;
```

```
        end
%         line([x0,x],[y0,y],[z,z]);
    end

end
% hold off
vz1=vz;


end
```

*zsfield.m*:

```
function[fieldsout] = zsfield(xvec,Ibias,Iprofile,Icomp1,Icomp2)
%outputs the values of the magnetic field, in Gauss, at points in xvec
%along the Zeeman slower axis

wirediameter = 1*10^-3;
tubeRadius = 0.02; %outer radius of slower tube

%%wire windings for bias field and profile field. Windings are given as
%%{number across, number high}
windingsBias = [420 1];
windingsProfile = {{15, -6},{10, -5},{50, -4},{70, -3},{65, -2},{60, -1},...
    {45,0},{40, 1},{20, 2},{15, 3},{10, 4},{10, 5},{10, 6}};
windingsComp1 = [8 5];
windingsComp2 = [8 5];

xZSend = 0.42; %end of ZS windings (despite 40 cm nominal ZS length)
rMOT = 92.265e-3; %distance from start of flange to MOT center
ZSMOTdist = 0.07; %length of tube between ZS and MOT chamber flange
xMOT = xZSend + ZSMOTdist + rMOT;
comp1Radius = 0.04;
comp2Radius = 0.03;
comp1start = xZSend + ZSMOTdist - 0.02 - windingsComp1(1)*wirediameter;
comp2start = xMOT + rMOT + 0.02;

%%calculation of fields

fieldsout = zeros(1,length(xvec));

for k = 1:length(xvec)
    x = xvec(k);

xstart = 0;
tuberadius = tubeRadius + wirediameter*windingsBias(2);
%adjusts inner radius for coils on top of bias to include bias windings

coilfieldsBias = zeros(1,windingsBias(1)*windingsBias(2));
for i = 1:windingsBias(1)
    for j = 1:windingsBias(2)
        coilfieldsBias((i-1)*windingsBias(2)+j) = BLoop(x,...
            xstart+(i-1/2)*wirediameter,Ibias,tubeRadius+(j-1/2)*wirediameter);
    end
end

```

```
%calculate number of windings and preallocate vector of fields
windingblocksProfile = zeros(1,length(windingsProfile));
for n = 1:length(windingsProfile)
    windingblocksProfile(n) = abs(windingsProfile{n}{1}*windingsProfile{n}{2});
end
nwindingsProfile = sum(windingblocksProfile);
coilfieldsProfile = zeros(1,nwindingsProfile);

xbegin = xstart;
count = 1;
for n = 1:length(windingsProfile)
    for i = 1:windingsProfile{n}{1}
        for j = 1:abs(windingsProfile{n}{2})
            if windingsProfile{n}{2} >= 0
                coilfieldsProfile(count) = BLoop(x,...
                    xbegin+(i-1/2)*wirediameter,Iprofile,...
                    tuberadius+(j-1/2)*wirediameter);
            else
                coilfieldsProfile(count) = -BLoop(x,...
                    xbegin+(i-1/2)*wirediameter,Iprofile,...
                    tuberadius+(j-1/2)*wirediameter);
            end
            count = count+1;
        end
    end
    xbegin = xbegin + wirediameter*windingsProfile{n}{1};
end

coilfieldsComp1 = zeros(1,windingsComp1(1)*windingsComp1(2));
for i = 1:windingsComp1(1)
    for j = 1:windingsComp1(2)
        coilfieldsComp1((i-1)*windingsComp1(2)+j) = BLoop(x,...
            comp1start+(i-1/2)*wirediameter,Icomp1,comp1Radius+(j-1/2)*wirediameter);
    end
end

coilfieldsComp2 = zeros(1,windingsComp2(1)*windingsComp2(2));
for i = 1:windingsComp2(1)
    for j = 1:windingsComp2(2)
        coilfieldsComp2((i-1)*windingsComp2(2)+j) = BLoop(x,...
            comp2start+(i-1/2)*wirediameter,Icomp2,comp2Radius+(j-1/2)*wirediameter);
    end
end

fieldsout(k) = sum([coilfieldsProfile coilfieldsBias coilfieldsComp1...
    coilfieldsComp2]);

end

end
```

*zsideal.m*:

```
function[fieldsout] = zsideal(xvec,eta,detuning)
%outputs ideal ZS field for a given security factor and laser detuning
%(detuning in MHz)
```

```
4
5  muB = 9.27401*10^-24;
6  mexc = -7;
7  ge = 1.160;
8  mg = -6;
9  gg = 1.1638;
10 muprime = (mexc*ge-mg*gg)*muB;
11
12 x0 = 0.4; %length of ZS
13 amax = 552786.1;
14 aZS = eta*amax;
15 vc = sqrt(2*aZS*x0);
16
17 hbar = 1.0545718*10^-34;
18 k401 = 2*pi/(400.91*10^-9);
19
20 deltaomega = 2*pi*detuning*10^6;
21 Bb = hbar/muprime*deltaomega*10^4;%Gauss
22 B0 = hbar*k401/muprime*vc*10^4;%Gauss
23
24 fieldsout = zeros(1,length(xvec));
25 for i = 1:length(xvec)
26     x = xvec(i);
27
28     if 0 <= x && x <= x0
29         fieldsout(i) = Bb + B0*sqrt(1-x/x0);
30     else
31         fieldsout(i) = 0;
32     end
33
34 end
35
36 end
```

*PopulationGrid.m*:

```
1  classdef PopulationGrid
2      properties
3          MaxValues
4          Populations
5          Detuning
6          Correction
7      end
8      methods
9          function obj = PopulationGrid(pop,maxval,det,cor)
10             if nargin == 4
11                 obj.MaxValues = maxval;
12                 obj.Populations = pop;
13                 obj.Detuning = det;
14                 obj.Correction = cor;
15             else
16                 obj.MaxValues = [0,0,0,0];
17                 obj.Populations = zeros(2,2,2,2);
18                 obj.Detuning = 0;
19                 obj.Correction = 0;
20             end
```

```
        end
    end
end
```

*OvenAtoms.m*:

```
classdef OvenAtoms
    properties
        Atoms
        Toven
        Thl
        Dap1
        Dap2
        Lap1
        Lap2
        Lhl
        THmax
        RateOut
        RateDepIn
        RateDepOut
        C1
        C2
    end
    methods
        function obj = OvenAtoms(atoms,t1,t2,d1,d2,l1,l2,l3,th,r1,r2,r3,c1,c2)
            if nargin == 14
                obj.Atoms = atoms;
                obj.Toven = t1;
                obj.Thl = t2;
                obj.Dap1 = d1;
                obj.Dap2 = d2;
                obj.Lap1 = l1;
                obj.Lap2 = l2;
                obj.Lhl = l3;
                obj.THmax = th;
                obj.RateOut = r1;
                obj.RateDepIn = r2;
                obj.RateDepOut = r3;
                obj.C1=c1;
                obj.C2=c2;
            else
                obj.Atoms = 0;
                obj.Toven = 0;
                obj.Thl = 0;
                obj.Dap1 = 0;
                obj.Dap2 = 0;
                obj.Lap1 = 0;
                obj.Lap2 = 0;
                obj.Lhl = 0;
                obj.RateOut = 0;
                obj.RateDepIn = 0;
                obj.RateDepOut = 0;
                obj.THmax=0;
                obj.C1=0;
                obj.C2=0;
            end
```

```
51          end
52      end
53  end
```

# Appendix B

# Analysis of the Pumping System Design

## B.1 Molecular Flow Regime

At very low pressures, when the mean free path is much larger than the average intermolecular distance, gasses are in the so called *molecular flow* regime. In this case it is possible to establish an equivalence between systems with gaseous flow and electrical circuits:

$$\text{Pressure} \longleftrightarrow \text{Voltage}$$
$$\text{Molecular Conductivity} \longleftrightarrow \text{Electrical Conductivity}$$
$$\text{Molecular Throughput} \longleftrightarrow \text{Electrical Current}$$

The molecular throughput is defined as $Q = p\dot{V}$, i.e. as pressure multiplied by the volumetric flow rate. For ideal gases it is proportional to the number flow rate, where the constant of proportionality is $k_B T$. The molecular conductivity of a chamber section is then defined as

$$C = \frac{Q}{\Delta p} \tag{B.1}$$

where $\Delta p$ is the pressure difference across the section, and $Q$ is the molecular throughput through that section. The conductance has units of *voulme/time*.In complex vacuum systems, involving chamber sections connected in parallel or in series, the effective conductance can be calculated using the formulas:

$$C_{par} = C_1 + C_2 \tag{B.2}$$
$$C_{ser} = \left(C_1^{-1} + C_2^{-1}\right)^{-1} \tag{B.3}$$

These formulas assume that the initial conditions for the atoms entering all chamber sections correspond to those of a large reservoirs. Care must be taken when applying these formulas to real chambers, as the quality of approximation might vary.

Some useful formulas for conductivities of relevant structures:

- Aperture:

$$C_{ap} = \sqrt{\frac{k_B T}{2\pi M}} A = C_0 A \tag{B.4}$$

  where $A$ is the surface area of the aperture, and $M$ is the molecular mass. Using this result, the conductivities of many pipe systems can be expressed using the *transmission probability*, $\alpha$:

$$C_{sys} = \alpha C_0 A \tag{B.5}$$

- Straight pipe section:
  A good approximation for $\alpha$ through a tube of diameter $D$ and length $L$ is:

$$\alpha = \frac{1}{1 + \frac{3L}{4D}} \tag{B.6}$$

  leading to the overall conductivity of :

$$C_{pipe} = \sqrt{\frac{\pi k_B T}{18M}} \frac{\frac{D^3}{L}}{1 + \frac{3L}{4D}} \tag{B.7}$$

- Elbow:
  A reasonably good approximation for $\alpha$ that matches the experimental results (ref) well is

$$\alpha = \frac{1}{1 + \frac{3}{8}\left(\frac{L_1}{D} + \frac{L_2}{D} + \frac{L_1 L_2}{(L_1 + L_2)D}\right)} \tag{B.8}$$

  where $L_1$ and $L_2$ are the lengths of the two branches of the elbow.

- Tee: An approximation applied in this case is using the series conductivity of the two straight branches for the straight section, and the conductivity of the elbow reduced by the conductivity of one of the straight branches for the orthogonal section.

Finally, in this picture, the vacuum pumps are modelled as connections to the *electrical ground*, i.e. zero pressure, through a conductance equal to the pumping speed of the pumps.

## B.2 Gas Sources

The reason behind the existence of an equilibrium pressure value in pumped vacuum systems are sources of gaseous material. In our case the three dominant contributors are leaks at the flange connections, outgassing from surfaces and gas permeation through the chamber.

- **Leaks**: In our apparatus, all the flange connections are made using the *Con Flat* (CF) flanges. Different manufacturers give varying specifications for leak rates od a properly sealed flange, but based on a range of sources, a good estimate seems to be $10^{-11}$ $mbar\ l\ s^{-1}$ per flange connection. This total rate is then distributed among components present in air according to partial pressures.

- **Outgassing**: Stainless steel has significant amounts of hydrogen dissolved, which leads to outgassing into the vacuum chamber. For 304L/316LN stainless steel, the outgassing rate for hydrogen is $10^{-12}$ $mbar\ l\ s^{-1}\ cm^{-2}$. Another possible source of significant outgassing is the Viton ring in the HV section valve, which lets out carbon monoxide. We have used the total rate of $10^{-9}$ $mbar\ l\ s^{-1}$ to account for this.

- **Permeation**: According to the literature, permeation of Hydrogen through stainless steel is a significant contributor only at very high temperatures. At room temperature, it is only necessary to account for Helium permeation through glass windows. The rate used, for glass of thickness $d$ is $3.8 \cdot 10^{-3}$ $mbar\ l\ s^{-1}\ cm^{-2}\ \left(\frac{d}{1mm}\right)^{-1}$

## B.3 Calcualtions for Our Experiment

Accounting for all the conductivities and rates (Figure B.1 and Table B.1) and solving the equivalent circuit, the final pressure in the chamber is estimated to be $2.410^{-11} mbar$ in the MOT chamber and $7.4 \cdot 10^{-12} mbar$ in the science cell.

| Gas | $Q_0$ | $Q_1$ | $Q_2$ | $Q_3$ | $Q_4$ | $Q_5$ | $Q_6$ | $Q_7$ | $Q_8$ | $Q_9$ | $S_2$ | $S_6$ | $S_9$ |
|---|---|---|---|---|---|---|---|---|---|---|---|---|---|
| | $[10^{-11}\ mbar\ l\ s^{-1}]$ | | | | | | | | | | | $[l\ s^{-1}]$ | |
| $N_2$ | 0.78 | 7.80 | 2.34 | 2.34 | 0.78 | 11.0 | 2.34 | 5.50 | 0.78 | 0.78 | 40 | 100 | 40 |
| $O_2$ | 0.21 | 2.1 | 0.63 | 0.63 | 0.21 | 2.9 | 0.63 | 1.5 | 0.21 | 0.21 | 100 | 300 | 100 |
| $Ar$ | 0.01 | 0.1 | 0.03 | 0.03 | 0.01 | 0.14 | 0.03 | 0.07 | 0.01 | 0.01 | 6 | 6 | 6 |
| $H_2$ | 48 | 48 | 25 | 16 | 6.7 | 63 | 40 | 50 | 0 | 6.7 | 100 | 300 | 100 |
| $He$ | 0 | 1.1 | 0 | 0 | 0 | 0.99 | 0.16 | 0.16 | 0.91 | 0 | 6 | 6 | 6 |
| $CO$ | 0 | 0 | 0 | 0 | 100 | 0 | 0 | 0 | 0 | 0 | 70 | 200 | 70 |

Table B.1 Leak rates and pumping speeds used in the calcualtions

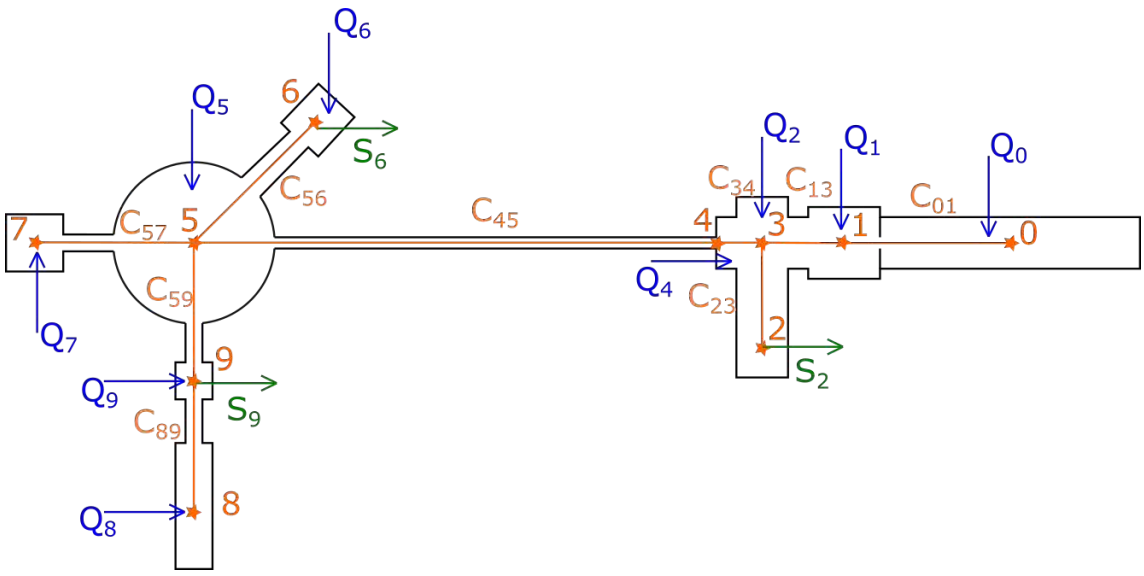


Fig. B.1 Sketch of the pumping system

# Appendix C

# Self-Heterodyne Linewidth Measurement

A standard technique for determining the linewidth of a single frequency laser is the delayed self-heterodyne linewidth measurement. It relies on the result that the frequency spectrum of intensity fluctuations of a signal obtained by interfering the laser light with itself and introducing a delay between the two components, will contain information about the laser linewidth. We have implemented this method using the setup shown in Figure C.1. A 2km long optical fibre is used to introduce a delay of $\tau_D = \frac{nL}{c} \approx 10\mu s$ into one of the two branches of the system. The other branch goes through an AOM[1] in order to introduce a $\Omega = 2\pi \cdot 110MHz$ frequency shift into the beam. Interfering the two peaks and recording the spectrum reveals a peak with oscillating tails centered around $\Omega$.

In order to extract information about the linewidth from the obtained spectrum, we have to analyse the functional form of the signal. The electrical field of the laser can be represented as:

$$E(t) = E_0 e^{i(\omega_0 t + \phi(t))} \tag{C.1}$$

where $\phi(t)$ represents the phase fluctuations. The electrical field in the interfered signal is:

$$E_\tau(t) = E(t) + \alpha E(t + \tau_D) e^{i\Omega t} \tag{C.2}$$

The photo-diode measures the light intensity, that is proportional to $|E_\tau|^2$, and the power spectrum of that quantity can be evaluated using the Wiener-Knichine theorem to be the Fourier transform of the autocorrelation function of the intensity, which is given by:

[1] Gooch & Housego AOMO 3110-197, 110MHz Acusto-Optic Modulator

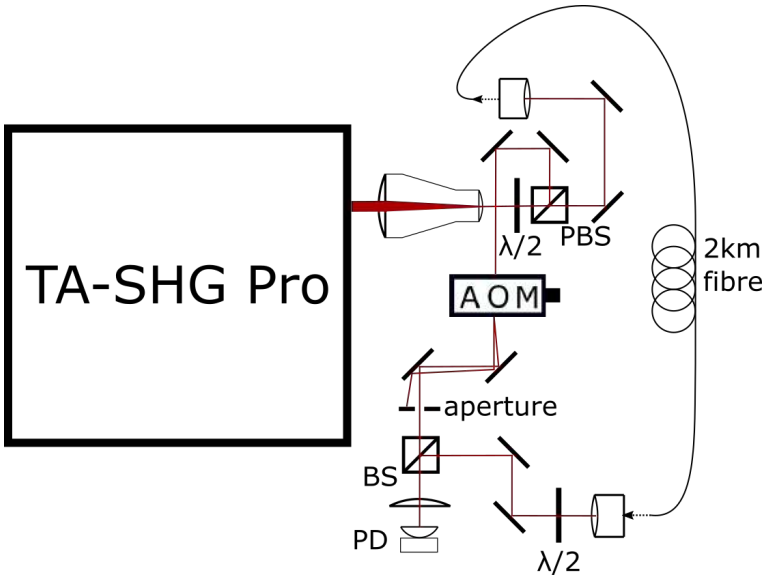


Fig. C.1 Delayed self heterodyne linewidth measurement setup

$$G^{(2)}_{E_\tau}(t') = \langle E_\tau(t) E^*_\tau(t) E_\tau(t+t') E^*_\tau(t+t') \rangle \tag{C.3}$$

By substituting the expression for $E_\tau$ and tidying up, one can obtain:

$$G^{(2)}_{E_\tau}(t') = E_0^4 \left[ (1+\alpha^2)^2 + 2\alpha^2 e^A \cos \Omega t' \right] \tag{C.4}$$

where the exponent is:

$$A = -\langle \Delta\phi^2(\tau_D) \rangle - \langle \Delta\phi^2(t') \rangle + \frac{1}{2} \langle \Delta\phi^2(\tau - \tau_D) \rangle + \frac{1}{2} \langle \Delta\phi^2(\tau + \tau_D) \rangle \tag{C.5}$$

and

$$\langle \Delta\phi^2(t') \rangle = \left\langle (\phi(t+t') - \phi(t))^2 \right\rangle \tag{C.6}$$

is the mean square phase fluctuation of the electric field. From [31] it is possible to relate the phase fluctuations to the frequency noise spectrum $S_f(\omega)$:

$$\langle \Delta\phi^2(t') \rangle = \frac{2}{\pi} \int_{-\infty}^{\infty} \sin^2\left(\frac{\omega t'}{2}\right) S_f(\omega) \frac{d\omega}{\omega^2} \tag{C.7}$$

In case of white-frequency noise spectrum, $S_f(\omega) = S_0$ it is possible to calculate the power spectrum of the measured intensity explicitly:

$$
\begin{aligned}
S(\omega) =& E_0^4 \{ \left(1+\alpha^2\right)^2 \delta(\omega) + 2\alpha^2 e^{-S_0\tau_D} \delta(\omega-\Omega) + \\
& 2\alpha^2 \frac{2S_0}{S_0^2+(\omega-\Omega)^2} \cdot \left[ 1 - e^{-S_0\tau_D} \left( \cos((\omega-\Omega)\tau_D) + \frac{S_0}{\omega-\Omega} \sin((\omega-\Omega)\tau_D) \right) \right] \}
\end{aligned}
\tag{C.8}
$$

# Appendix D

# Issues with Trapping the Fermionic Isotope in the 1064 nm ODT

We suspect that the reason behind reported poor lifetimes of the fermionic $^{167}Er$ isotope in a 1064nm Optical Dipole Trap is the existence of an electronic state at 1069.5 nm. That state has J=8 making the transition dipole forbidden from the ground state (J=6) for bosonic isotopes. But since the fermionic isotope has I=7/2, there seems to exist dipole allowed transitions to this state, that does not break the $\Delta F \leq 1$ transition rule. An example would be:

$$\left| g; J=6, I=\frac{7}{2}, F=\frac{19}{2}, m_F=\frac{19}{2} \right\rangle \rightarrow \left| e; J=8, I=\frac{7}{2}, F=\frac{21}{2}, m_F=\frac{21}{2} \right\rangle \tag{D.1}$$

# References


[1] Steven Chu, L. Hollberg, J. E. Bjorkholm, Alex Cable, and A. Ashkin. Three-dimensional viscous confinement and cooling of atoms by resonance radiation pressure. *Phys. Rev. Lett.*, 55:48–51, Jul 1985.

[2] M. H. Anderson, J. R. Ensher, M. R. Matthews, C. E. Wieman, and E. A. Cornell. Observation of bose-einstein condensation in a dilute atomic vapor. *Science*, 269(5221):198–201, 1995.

[3] K. B. Davis, M. O. Mewes, M. R. Andrews, N. J. van Druten, D. S. Durfee, D. M. Kurn, and W. Ketterle. Bose-einstein condensation in a gas of sodium atoms. *Phys. Rev. Lett.*, 75:3969–3973, Nov 1995.

[4] B. DeMarco and D. S. Jin. Onset of fermi degeneracy in a trapped atomic gas. *Science*, 285(5434):1703–1706, 1999.

[5] Axel Griesmaier, Jörg Werner, Sven Hensler, Jürgen Stuhler, and Tilman Pfau. Bose-einstein condensation of chromium. *Phys. Rev. Lett.*, 94:160401, Apr 2005.

[6] K. Aikawa, A. Frisch, M. Mark, S. Baier, A. Rietzler, R. Grimm, and F. Ferlaino. Bose-einstein condensation of erbium. *Phys. Rev. Lett.*, 108:210401, May 2012.

[7] Mingwu Lu, Nathaniel Q. Burdick, Seo Ho Youn, and Benjamin L. Lev. Strongly dipolar bose-einstein condensate of dysprosium. *Phys. Rev. Lett.*, 107:190401, Oct 2011.

[8] Alexander L. Gaunt, Tobias F. Schmidutz, Igor Gotlibovych, Robert P. Smith, and Zoran Hadzibabic. Bose-einstein condensation of atoms in a uniform potential. *Phys. Rev. Lett.*, 110:200406, May 2013.

[9] Nir Navon, Alexander L. Gaunt, Robert P. Smith, and Zoran Hadzibabic. Critical dynamics of spontaneous symmetry breaking in a homogeneous bose gas. *Science*, 347(6218):167–170, 2015.

[10] Christoph Eigen, Alexander L. Gaunt, Aziza Suleymanzade, Nir Navon, Zoran Hadzibabic, and Robert P. Smith. Observation of weak collapse in a bose-einstein condensate. *Phys. Rev. X*, 6:041058, Dec 2016.

[11] Nir Navon, Alexander Gaunt, Robert Smith, and Zoran Hadzibabic. Emergence of a turbulent cascade in a quantum gas. *Nature*, 539, Sep 2016.

[12] Albert Frisch. *Dipolar Quantum Gases of Erbium*. PhD thesis, University of Innsbruck, 2014.

[13] L. Chomaz, R. M. W. van Bijnen, D. Petter, G. Faraoni, S. Baier, J. H. Becher, M. J. Mark, F. Wächtler, L. Santos, and F. Ferlaino. Observation of roton mode population in a dipolar quantum gas. *Nature Physics*, 14:442–446, May 2018.

[14] Adam Bühler and Hans Peter Büchler. Supersolid phase in atomic gases with magnetic dipole interaction. *Phys. Rev. A*, 84:023607, Aug 2011.

[15] J. H. Becher, S. Baier, K. Aikawa, M. Lepers, J.-F. Wyart, O. Dulieu, and F. Ferlaino. Anisotropic polarizability of erbium atoms. *Phys. Rev. A*, 97:012509, Jan 2018.

[16] Albert Frisch, Michael Mark, Kiyotaka Aikawa, Francesca Ferlaino, John L Bohn, Constantinos Makrides, Alexander Petrov, and Svetlana Kotochigova. Quantum chaos in ultracold collisions of gas-phase erbium atoms. 507:475–9, 03 2014.

[17] Johannes Schindler. Characterization of an erbium atomic beam. Master's thesis, University of Innsbruck, 2011.

[18] Thomas Maier. *Interactions in a Quantum Gas of Dysprosium Atoms*. PhD thesis, University of Stuttgart, 2015.

[19] Tobias Schaich. *A Tunable Optical Dipole Trap for Erbium*. Part III Project Report, University of Cambridge, 2018.

[20] D J McCarron, S A King, and S L Cornish. Modulation transfer spectroscopy in atomic rubidium. *Measurement Science and Technology*, 19(10):105601, 2008.

[21] Julian Léonard, Moonjoo Lee, Andrea Morales, Thomas M Karg, Tilman Esslinger, and Tobias Donner. Optical transport and manipulation of an ultracold atomic cloud using focus-tunable lenses. *New Journal of Physics*, 16(9):093028, 2014.

[22] Nathaniel Vilas. Laser cooling of erbium. Master's thesis, University of Cambridge, 2018.

[23] Aviv Keshet. http://akeshet.github.io/cicero-word-generator/.

[24] Aziza Suleymanzade. Ultracold atoms experiment for trapping $^{39}k$ in an optical box trap. Master's thesis, University of Cambridge, 2014.

[25] Kevin M. Birnbaum. *Cavity QED with Multilevel Atoms*. PhD thesis, California Institute of Technology, 2005.

[26] A. Chambers, R. K. Fitch, and B. S. Halliday. *Basic Vacuum Technology*. IoP, 2nd edition, 1998.

[27] John L. Hall, Matthew S. Taubman, and Jun Ye. *Handbook of Optics, Chapter 27:Laser Stabilisation*. McGraw-Hill, 2nd edition, 2004.

[28] Tanish Satoor. *Towards Laser Cooling of Erbium Atoms*. Part III Project Report, University of Cambridge, 2018.

[29] Bogna Bylicka, Dariusz Chruscinski, and S. Maniscalco. Non-markovianity and reservoir memory of quantum channels: a quantum information theory perspective. In *Scientific reports*, 2014.

[30] Ji-Bing Yuan, Hai-Jun Xing, Le-Man Kuang, and Su Yi. Quantum non-markovian reservoirs of atomic condensates engineered via dipolar interactions. *Phys. Rev. A*, 95:033610, Mar 2017.

[31] L. B. Mercer. 1/f frequency noise effects on self-heterodyne linewidth measurements. *Journal of Lightwave Technology*, 9(4):485–493, Apr 1991.